Heme drives hemolysis-induced susceptibility to infection and sepsis via disruption of phagocyte cytoskeletal dynamics

Rui Martins[1,2], Julia Maier[1,2], Anna-Dorothea Gorki[1,2], Kilian V. M. Huber[1], Omar Sharif[1,2], Philipp Starkl[1,2], Simona Saluzzo[1,2], Federica Quattrone[1,2], Riem Gawish[1,2], Karin Lakovits[2], Michael C. Aichinger[3], Branka Radic-Sarikas[1], Charles-Hugues Lardeau[1], Anastasiya Hladik[1,2], Ana Korosec[1,2], Markus Brown[4], Kari Vaahtomeri[5], Michelle Duggan[5], Dontscho Kerjaschki[4], Harald Esterbauer[6], Jacques Colinge[1], Stephanie C. Eisenbarth[7], Thomas Decker[3], Keiryn L. Bennett[1], Stefan Kubicek[1], Michael Sixt[5], Giulio Superti-Furga[1,8], and Sylvia Knapp[1,2]

[1] CeMM Research Center for Molecular Medicine of the Austrian Academy of Sciences, Vienna, Austria; [2] Department of Medicine I, Laboratory of Infection Biology, Medical University of Vienna, Vienna, Austria; [3] Max F. Perutz Laboratories, University of Vienna, Vienna, Austria; [4] Department of Pathology, Medical University of Vienna, Vienna, Austria; [5] IST Austria (Institute of Science and Technology Austria), Klosterneuburg, Austria; [6] Clinical Department of Medical and Chemical Laboratory Diagnostics, Medical University of Vienna, Vienna, Austria; [7] Department of Laboratory Medicine and Department of Immunobiology, Yale University School of Medicine, New Haven, USA; [8] Center for Physiology and Pharmacology, Medical University of Vienna, Vienna, Austria

Running title

Heme impairs host resistance to bacteria via interference with cytoskeleton dynamics.

Correspondence to:

Sylvia Knapp, MD, PhD

CeMM Research Center for Molecular Medicine of the Austrian Academy of Sciences, and

Department of Medicine I, Laboratory of Infection Biology, Medical University of Vienna

Waehringer Guertel 18-20, 1090 Vienna, Austria

Phone: +43-1-40400-51390; Fax: +43-1-40400-51670;

E-mail: sylvia.knapp@meduniwien.ac.at

Abstract

Hemolysis drives susceptibility to bacterial infections and predicts poor outcome from sepsis. These detrimental effects are commonly considered a consequence of heme-iron serving as a nutrient for bacteria. Here, we employed a Gram-negative sepsis model and found that elevated heme levels impaired the control of bacterial proliferation independent of heme-iron acquisition by pathogens. We demonstrate that heme strongly inhibited phagocytosis and migration of human and mouse phagocytes by disrupting actin cytoskeletal dynamics via DOCK8-triggered Cdc42 activation. A chemical screening approach revealed that quinine effectively prevented heme effects on the cytoskeleton, restored phagocytosis and improved survival in sepsis. These mechanistic insights provide potential therapeutic targets for patients with sepsis or hemolytic disorders.

Introduction

Intravascular hemolysis is a serious complication accompanying severe inflammatory conditions such as sepsis and an established complication of hemolytic disorders like sickle cell disease (SCD), malaria infection or beta-thalassemia, affecting millions of people worldwide[1, 2, 3, 4, 5]. In these disorders, extensive hemolysis leads to the release of the heme moiety from hemoglobin, which can rapidly exhaust the body's heme-scavenging capacity and result in high amounts of circulating heme[5, 6, 7, 8]. Excess heme is recognized as a central player in driving disease pathology, primarily due to its pro-oxidant properties that sensitize cells to the cytopathic effects of inflammatory mediators like TNF[9, 10, 11]. These effects have been demonstrated in models of polymicrobial sepsis and noncerebral malaria, in which mice lacking the heme-degrading enzyme HO-1 (heme oxygenase-1) have increased disease severity and succumb to organ failure[4, 12].

However, reduced disease tolerance cannot explain the significantly increased susceptibility to bacterial infections in people with hemolytic disorders like SCD[13], beta-thalassemia[14] or malaria[15, 16]. Mortality rates of 40% in children with SCD[1] reflect the tremendous threat of bacterial infections in these patients, and justify the current recommendation of prophylactic antibiotics until adolescence[17, 18]. In spite of the medical importance and apparent link between hemolysis and infection, most studies on heme have either employed sterile stimuli[19] or were performed in the presence of bactericidal antibiotics[4], effectively precluding the examination of heme effects on antibacterial effector mechanisms. Hemolysis is often considered a logical explanation for the increased rate of bacterial infections, because most pathogens depend on environmental iron sources, and heme is an iron-containing protoporphyrin (FePPIX)[20]. Recently, impaired neutrophil effector functions upon hemolysis were observed in humans with malaria[21] or beta-thalassemia[14], and in mouse models of malaria[22]. These studies have suggested a potential role for heme in modulating host resistance mechanisms. However, the mechanism of how excess heme precisely affects host immunity to bacteria remains elusive. Here we reveal that, contrary to previous interpretations, heme does not affect bacterial growth through nutrient availability. Instead, heme strongly suppresses phagocyte functions by inducing extensive actin cytoskeleton changes through interference with DOCK8-mediated Cdc42 activation, ultimately predisposing mice to bacterial dissemination and sepsis. Importantly, using a chemical screening approach, we provide a novel therapeutic proof-of-concept strategy aimed at restoring endogenous host resistance mechanisms.

74

Results

Heme impairs bacterial clearance *in vivo*

We sought to determine whether the extent of hemolysis would impact on host resistance mechanisms and consequently on bacterial burden during Gram-negative bacteria-induced sepsis. The number of bacteria present in the blood of septic mice infected with a pathogenic *Escherichia coli* strain (*E. coli,* strain PMV-1 used throughout this study) directly correlated with heme abundance in the plasma (**Fig. 1a**). To better understand the link between heme abundance and bacteremia severity, we pretreated mice with heme (25μmol/kg intraperitoneally (i.p.) for all heme treatments *in vivo*) to exogenously increase heme in the plasma, before infection with *E. coli* ($1x10^4$ CFU i.p.). While *E. coli* sepsis itself was accompanied by modest hemolysis, exogenous heme administration led to significantly increased plasma heme levels compared to PBS-treated mice, both 6 and 16h post-infection (**Fig. 1b**, **Supplementary Fig. 1a**). This was paralleled by a substantial increase in the bacterial burden in heme-treated mice (**Fig. 1c**, **Supplementary Fig. 1b**) and translated into a strongly impaired survival compared to PBS-treated mice (**Fig. 1d**).

Macrophages are crucial in the removal of excess heme resulting from hemolysis via the uptake and degradation of heme by HO-1[23], encoded by *Hmox1*. To address whether an increase in endogenous heme due to defective heme degradation in macrophages would negatively impact bacterial clearance during sepsis *in vivo*, we investigated *LysM*-$Cre^{+/-}$*Hmox1*$^{fl/fl}$, which lack expression of *Hmox1* in macrophages and neutrophils[24] and *LysM*-$Cre^{-/-}$*Hmox1*$^{fl/fl}$ littermates. Following i.p. *E. coli* infection, we observed a significant increase in plasma heme in *LysM*-$Cre^{+/-}$*Hmox1*$^{fl/fl}$ mice (**Fig. 1e**, **Supplementary Fig. 1c**), that was accompanied by increased bacterial numbers in blood and liver (**Fig. 1f, Supplementary Fig. 1d**) and impaired survival (**Fig. 1g**) when compared to *LysM*-$Cre^{-/-}$*Hmox1*$^{fl/fl}$ controls. Similar results were obtained in a separate model of infection with the unrelated Gram-positive pathogen *Listeria monocytogenes* (*L. monocytogenes*) (**Supplementary Fig. 1e-f**). To test potential pro-inflammatory effects of heme and to control for increased bacterial numbers in mice with high plasma heme during *E. coli*-induced sepsis, we challenged mice with LPS (40mg/kg i.p., 16h). Mice pretreated with heme had similar plasma IL-6 and TNF amounts and peritoneal KC and MCP-1 levels, as well as cell recruitment as mice pretreated with PBS (**Supplementary Fig**. **1g-i**), indicating that high plasma heme did not affect the inflammatory response. Thus, enhanced plasma heme, induced by

either exogenous heme administration or the lack of HO-1 expression in macrophages, resulted in an increased susceptibility to *E. coli* sepsis.

Independence of heme-iron acquisition

Upon infection, hosts reduce the bioavailability of iron through iron withdrawal, leading pathogenic bacteria to develop compensatory iron acquisition mechanisms[25]. We tested the importance of heme as an iron source for *E. coli* under limited iron availability *in vitro*. Chelation of growth-medium iron with deferoxamine (DFO, 10μM) led to a reduction in bacterial growth compared to non-chelated controls (**Fig. 2a**). This defect was not rescued by heme supplementation (**Fig. 2a**), suggesting that heme could not fully compensate for limited iron availability. Pathogenic *E. coli* are known to utilize several outer membrane heme transporters and periplasmic heme binding proteins to utilize heme as an iron source[26]. However, *E. coli* uses a single inner membrane ABC transporter, the dipeptide permease (DppBCDF), to import heme into the cytoplasm, and the deletion of any of its components renders *E. coli* unable to grow if heme is the only iron source[27]. To test if heme-iron provides a growth advantage to bacteria *in vivo*, we generated an isogenic mutant *E. coli* lacking the DppBCDF-subunit DppC (Δ*dppC::Kan*^{R}), which cannot utilize heme-iron (**Supplementary Fig. 1j**). We observed a severely increased bacterial load in the blood and livers of heme-treated wild-type mice 16h post-infection with Δ*dppC::Kan*^{R} compared to PBS-treated mice (**Fig. 2b, c**), suggesting that heme-iron acquisition could not explain the enhanced bacterial growth upon elevated heme concentrations. Next, we infected wild-type mice pretreated with PBS, heme or an equimolar amount of free iron (ferric ammonium citrate, Fe^{3+}) with wild-type *E. coli*. Plasma heme amounts were comparable in mice pretreated with Fe^{3+} or PBS (**Fig. 2d**), and despite the similarly increased availability of iron in both heme- and Fe^{3+}-treated mice (**Fig. 2e**), only heme-treated mice presented a significantly higher bacterial burden in the blood and liver compared to PBS or Fe^{3+}-treated mice (**Fig. 2f**). Similar results were obtained in mice infected with *L. monocytogenes* (**Supplementary Fig. 1k**). These results indicate that heme directly leads to increased bacterial counts during sepsis, and that bacterial iron requirements are met via heme-independent mechanisms.

The secretion of hemolytic toxins by pathogenic bacteria is an important virulence factor, currently considered as a means of enhancing the availability of iron for bacteria[25]. To understand

the contribution of bacterial hemolysins to hemolysis and bacterial infection, and because the *E. coli* strain (PMV-1) used in our study does not secrete hemolysins, we used Tn7 transposition to introduce a single copy of the *E. coli* alpha-hemolysin operon from strain CFT073 into the genome of PMV-1 *E. coli*, to generate hemolytic *E. coli*$^{hlyABCD::attTn7}$ (**Supplementary Fig. 1l**). Infection of wild-type mice with *E. coli*$^{hlyABCD::attTn7}$ further increased heme plasma concentrations (**Fig. 2g**), and resulted in elevated bacterial counts compared to infection with wild-type *E. coli* (**Fig. 2h**), showing that pathogen-induced hemolysis is an important virulence mechanism to evade host resistance. Together, these data show that bacteria exploited the inflammation- and/or hemolysin-triggered release of heme independently of iron acquisition.

Heme potently inhibits phagocytosis

Next, we investigated how heme influenced host resistance mechanisms responsible for restricting bacterial growth. We focused on macrophage effector functions and found that heme pretreatment (15min, 3-30μM throughout this study, unless otherwise indicated) led to a strong, dose-dependent reduction of phagocytosis of *E. coli* by RAW264.7 macrophages compared to DMSO-treated controls (**Fig. 3a-b, Supplementary Fig. 2a**). Neither hemoglobin, free iron, nor the heme analogs tin-protoporphyrin IX (SnPPIX) or protoporphyrin IX (PPIX) suppressed bacterial phagocytosis by RAW264.7 macrophages at heme-equivalent concentrations (**Supplementary Fig. 2b-e**). Notably, heme did not alter bacterial binding or bacterial killing by macrophages (**Supplementary Fig. 3f-g**). Incubation of murine primary peritoneal macrophages, bone marrow-derived macrophages (BMDM) and neutrophils with heme led to a similar reduction of phagocytosis of *E. coli*, *Pseudomonas aeruginosa*, *Streptococcus pneumoniae* and *L. monocytogenes* (**Fig. 3c-d, Supplementary Fig. 2h-k**), and heme strongly suppressed bacterial phagocytosis by human monocyte-derived macrophages (**Fig. 3e**, **Supplementary Fig. 2l**) and neutrophils (**Fig. 3f**), compared to DMSO controls. Additionally, we observed that heme treatment of RAW264.7 macrophages led to a dose-dependent inhibition of apoptotic cell uptake (**Supplementary Fig. 2m**).

To assess the physiological impact of heme-induced inhibition of phagocytosis in the tissue most relevant for hemolysis, we measured bacterial phagocytosis in human whole blood. Induction of hemolysis with phenylhydrazine or addition of heme to whole blood at concentrations mimicking the physiological range of plasma heme in hemolytic patients (5-50μM)[6], led to a dose-dependent

impairment of *E. coli* phagocytosis by neutrophils and monocytes compared to DMSO controls (**Fig. 3g, Supplementary Fig. 2n-o**), indicating our mouse model is reflective of human hemolytic conditions. To test if heme-related cytotoxicity[11] caused the inhibition of phagocytosis, we pre-incubated RAW264.7 macrophages with heme (15min), and washed the cells before addition of bacteria. Removal of heme by washing induced a complete recovery of the phagocytic capacity of macrophages compared to those where heme was not removed (**Fig. 3h**), indicating that cell viability was not compromised. In addition, heme only mildly induced cell death at 30μM (**Fig. 3i, Supplementary Fig. 2p**), as previously reported for macrophages[11].

To test whether heme affected macrophage phagocytosis *in vivo*, wild-type mice pretreated with PBS or heme were injected i.p. with FITC-labeled heat-killed *E. coli* (FITC-*E. coli*). We found a strong reduction in the percentage of phagocytosing ($FITC^+$) $F4/80^+CD11b^+Ly6G^-$ peritoneal macrophages of heme-treated versus PBS-treated mice (**Fig. 3j**). Reduced *in vivo* phagocytosis was also observed in cytospin preparations of peritoneal exudate cells from mice treated with heme, as compared to PBS, and infected with live *E. coli* to induce sepsis (**Fig. 3k**). These results show that heme inhibition of phagocytosis occurred at sub-toxic levels and required the intact heme molecule.

Heme disrupts actin cytoskeleton dynamics

Phagocytosis of pathogens relies on a tightly regulated actin cytoskeleton rearrangement following recognition of foreign bodies, and any interference with its regulation negatively impacts host resistance against bacteria[28]. Concordantly, we found that exposure of RAW264.7 and human monocyte-derived macrophages to heme led to changes in cell shape, accompanied by cell spreading and a strong induction of filopodia formation (**Fig. 4a-b, Supplementary Video 1**), which was visible within three minutes of stimulation with heme but not with DMSO or PPIX (**Fig. 4c**, **Supplementary Fig. 3a, Supplementary Videos 2-3**). We quantified these changes by automatic image analysis and revealed that heme-induced cytoskeleton rearrangement led to a significant increase in cell area and perimeter, as well as a decrease in circularity (form factor) (**Fig. 4d-e**, **Supplementary Fig. 3b-d**), indicating that the heme-induced defective phagocytic response is likely tied to cytoskeleton rearrangements.

During immune responses against bacteria, cytoskeletal rearrangement is required beyond phagocytosis and is crucial for cell recruitment and migration[29]. To investigate if heme had additional effects, we employed a wound-healing assay and found that heme dose-dependently hampered the motility of BMDM when compared to DMSO-treatment (**Fig. 5a-b**). Similarly, mouse bone marrow-derived dendritic cell migration in a 3D collagen gel towards a CCL19 gradient was impaired in the presence of heme, compared to DMSO control (**Fig. 5c-d, Supplementary Video 4**). In addition, rolling and adhesion of primary human monocytes onto a TNF-activated endothelial layer under flow conditions, which rely on actin polymerization to stabilize integrin anchors onto the endothelium[30], were impaired by addition of heme compared to DMSO-treated controls (**Supplementary Fig. 4a-b, Supplementary Video 5**).

In vivo, both heme-treated wild-type or *LysM*-Cre$^{+/-}$*Hmox1*$^{fl/fl}$ mice exhibited no increase in peritoneal cell influx 6h post-infection with *E. coli* when compared to PBS-treated or *LysM*-Cre$^{-/-}$*Hmox1*$^{fl/fl}$ controls, respectively, (**Supplementary Fig. 4c-d**) despite higher peritoneal chemokine concentrations (KC and MCP-1; **Supplementary Fig. 4e-f**). Furthermore, employing a thioglycollate-induced peritonitis model, we found neutrophil migration disrupted in heme- as compared to PBS-treated mice *in vivo* (**Supplementary Fig. 4g-i**). Together, these data show that heme induced extensive actin cytoskeleton alterations, resulting in defective phagocytosis and inflammatory cell migration.

Heme activates Cdc42 via DOCK8

Heme is an amphipathic molecule, which can promote the generation of reactive oxygen species (ROS) via Fenton chemistry, thereby leading to membrane damage[31]. As such, the actin cytoskeleton rearrangement induced by heme could be triggered by calcium influx upon membrane damage, receptor-signaling or ROS sensing. Heme-treated RAW264.7 macrophages cultured in the absence of extracellular calcium or in the presence of a ROS scavenger showed cytoskeleton remodeling similar to heme-treated positive controls (**Supplementary Fig. 5a-d**), indicating that heme-induced effects on the cytoskeleton were independent of ROS or receptor-triggered calcium signaling.

To decipher the signaling pathways underlying the cytoskeleton changes induced by heme, we incubated lysates of RAW264.7 macrophages with control (empty) or heme-agarose beads and

identified binding proteins by liquid chromatography-mass spectrometry (**Supplementary Fig. 6a**). High-affinity interactions were discriminated from abundant or low-affinity interactions by competition with free heme. Binding proteins were scored according to their affinity to heme using the algorithms SAINT[32] and CRAPome[33], as well as the fold reduction in spectral counts upon competition with excess heme (**Fig. 6a**). Using the STRING database of known and predicted protein-protein interactions[34], we retrieved an interaction network involving various proteins known to interact with, or activate the small GTPase Cdc42, an intracellular signaling regulator, as well as members of the ARP2/3 and WAVE actin cytoskeleton regulator complexes (**Fig. 6a-b**). The heme-association of several candidate proteins in this network was validated by affinity purification with heme-agarose beads followed by western blotting (**Fig. 6c**).

Cdc42 is involved in cell motility and phagocytosis, but is mainly recognized as a central node in the formation of lamellipodia and filopodia at the leading edge[35]. In line with the observation that heme-treated macrophages rapidly altered their cell shape and concomitantly formed numerous filopodia, we investigated whether heme led to the activation of Cdc42 and/or ARP2/3 in macrophages. Heme stimulation of RAW264.7 macrophages induced immediate Cdc42 activation for up to 30 minutes after stimulation (**Fig. 6d**), without changes in total Cdc42 protein amounts (**Supplementary Fig. 6b**). Selective inhibition of Cdc42 with ML141 effectively blocked all heme-induced changes in cell shape, and this effect could be reversed by removal of ML141 by washing prior to heme treatment (**Fig. 6e-f**, **Supplementary Fig. 6c-d**). Consistent with the essential role of ARP2/3 in the formation of lamellipodia[35], specific inhibition of the ARP2/3 complex with CK666 blocked heme-induced lamellipodia, but not filopodia formation (**Supplementary Fig. 6c, e-f**). As a control, CRISPR-targeted deletion of the cytoskeleton signaling protein MPP1 or the cell-adhesion mediator galectin 3 (LGALS3) in RAW264.7 macrophages, which we identified as heme-associated proteins not known to interact with Cdc42 (**Fig. 6b**), did not prevent heme-induced actin cytoskeleton reorganization compared to wild-type cells (**Supplementary Fig. 6g-h**). We therefore focused on Cdc42-induced filopodia formation, which can be elicited via the activation of the actin nucleator mDIA2[36]. Inhibiting mDIA2 using its specific inhibitor K216-0385, fully abrogated heme-induced filopodia extension (**Fig. 6g-h**, **Supplementary Fig. 6c**). DOCK8, a member of the atypical guanine nucleotide exchange factor (GEF) family reported to specifically activate Cdc42[37], was among the proteins with highest affinity to heme (**Fig. 6a-c**). To test the role of DOCK8 in mediating heme-induced actin cytoskeleton changes, we used BMDM generated from wild-type and *Dock8*$^{-/-}$ ER-HoxB8-

immortalized bone marrow progenitors. In contrast to wild-type ER-HoxB8 BMDM, *Dock8*$^{-/-}$ ER-HoxB8 BMDM did not spread or extend filopodia (**Fig. 7a-b**) and failed to activate Cdc42 upon treatment with heme (**Fig. 7c**), indicating that DOCK8 was essential for heme-induced activation of Cdc42. Of note, stimulation with the unrelated Cdc42 activator bradykinin led to cell shape changes in both wild-type and *Dock8*$^{-/-}$ ER-HoxB8 macrophages (**Supplementary Fig. 7a**), indicating that the lack of heme-induced filopodia extensions in the absence of DOCK8 was not due to intrinsic cytoskeletal defects. Consequently, *Dock8*$^{-/-}$ BMDM were protected from the inhibitory effect of heme on phagocytosis of *E. coli*, compared to their wild-type counterparts (**Fig. 7d, Supplementary Fig. 7b-c**). To assess whether DOCK8 deletion provided protection against the detrimental effects of heme on bacterial clearance during sepsis *in vivo*, we reconstituted lethally irradiated wild-type mice with wild-type or *Dock8*$^{-/-}$ bone marrow to generate WT>WT and *Dock8*$^{-/-}$>WT bone marrow chimeras. After successful engraftment, as verified by the percentage of donor (CD45.2^{+}) vs. recipient (CD45.1^{+}) leukocytes six weeks after reconstitution (**Supplementary Fig. 7d**), chimeric mice were treated with PBS or heme 30min before *E. coli* infection. In spite of similarly elevated plasma heme levels in WT>WT and *Dock8*$^{-/-}$>WT chimeras upon heme treatment (**Fig. 7e**), *Dock8*$^{-/-}$>WT chimeras were significantly protected against excess heme and showed a 10-fold reduction in bacterial numbers in liver, blood, and peritoneal cavity (**Fig. 7f**). These results indicated that heme acts via DOCK8 to activate Cdc42, leading to dysregulated actin polymerization and impaired bacterial clearance (**Supplementary Fig. 7e**).

Quinine restores phagocytosis *in vitro* and *in vivo*

Because inhibition of cytoskeletal effector molecules such as DOCK8 or Cdc42 is not amenable as a therapeutic strategy due to the potential inhibitory effects on cell migration and phagocytosis[38], we sought to identify suitable compounds that could prevent the heme-induced inhibition of phagocytosis without affecting baseline phagocytosis of bacteria. To do so, we employed an automated screening platform and tested 389 compounds, including a library representing the diversity of approved drugs regarding their chemical structures and molecular targets. We used high-throughput automated microscopy to measure the phagocytosis efficiency of RAW264.7 macrophages pretreated with the compound library and incubated with heme or DMSO (**Supplementary Fig. 8a**) and scored the compounds based on their efficacy at

preventing heme-induced inhibition of phagocytosis (**Fig. 8a**, **Supplementary Fig. 8b**). The top performing drug identified was the antimalarial compound quinine, which fully restored phagocytosis in the presence of heme, without affecting baseline phagocytosis (**Fig. 8a**, **Supplementary Fig. 8b-c**).

Quinine pretreatment protected RAW264.7 macrophages (**Fig. 8b, Supplementary Fig. 8c-d**) and human macrophages (**Fig. 8c**) from heme-induced inhibition of phagocytosis, and actin cytoskeleton changes (**Supplementary Fig. 8e-f**) compared to DMSO-treated cells. Importantly, quinine diminished the association of heme with DOCK8 without affecting the association of heme with MPP1 or LGALS3 in RAW264.7 macrophages (**Fig. 8d**), suggesting that quinine exerted its protective effect by specifically disrupting the heme-DOCK8 association. To test the effects of quinine *in vivo*, wild-type mice were pretreated with PBS or heme, followed by mock or quinine treatment (60mg/kg) before FITC-*E. coli* i.p. injection. Quinine treatment abrogated the inhibitory effect of heme on bacterial phagocytosis by peritoneal macrophages (**Fig. 8e**), indicating that quinine could also restore macrophage phagocytosis *in vivo*. Upon induction of *E. coli* peritonitis in wild-type mice, quinine treatment did not affect plasma heme levels but led to a reduction of bacterial counts in blood and liver (**Fig. 8f-g**, **Supplementary Fig. 8g-h**), thereby restoring the bacterial clearance capacity of heme-treated mice. Importantly, the dose of quinine used above did not affect bacterial growth *in vitro* (**Supplementary Fig. 8i-j**). Finally, quinine-treatment of heme-treated mice significantly improved survival compared to heme-treated mice, which received mock treatment (**Fig. 8h**), indicating quinine treatment prevented the detrimental effects of exogenous heme administration. Furthermore, quinine treatment also improved the survival of PBS-treated mice compared to mock-treatment of PBS-treated mice (**Fig. 8h**). These results indicate that quinine prevented the harmful effects of endogenously elevated heme in the course of Gram-negative bacteria-induced sepsis.

Discussion

Here we show that heme released in the course of hemolysis is a critical factor in driving bacterial outgrowth via the disruption of host resistance mechanisms by interfering with phagocyte cytoskeletal dynamics. Earlier observations of increased infection rates in the presence of iron, heme, hemoglobin and related compounds have commonly been ascribed to the nutritional benefit of increased iron availability for bacteria[20, 39]. In fact, iron withholding is a widely accepted immune mechanism to restrict bacterial growth by limiting iron bioavailability[40]. In line with the notion that all bacterial pathogens are able to circumvent nutritional immunity[25], our data indicate that the iron requirement for bacterial growth is met in the course of infection, independent of heme-iron acquisition by the pathogen *in vivo*.

Efficient pathogen removal greatly relies on phagocytosis by macrophages as a first line of defense[41]. Upon phagocytic receptor engagement, precise signaling triggers local cytoskeletal rearrangements allowing the engulfment of bacteria[28]. We discovered that this process is disrupted by excess heme, thereby creating a permissive host environment for bacterial infections and sepsis. Given the importance of phagocytosis, it is not surprising that pathogens have evolved means to avoid internalization, often by manipulating the host cell cytoskeleton[42]. In fact, some pathogens directly target Cdc42 activity to prevent phagocytosis in a manner analogous to our findings[42]. It is therefore conceivable that the evolution of erythrocyte-lysing toxins, such as alpha-hemolysin, provide an important means of evading host defense by inducing heme release. As such, our findings provide a new perspective on the role of these toxins during bacterial infections, independent from their proposed role as a means to increase iron availability. Another aspect to consider relates to the generation of bioactive molecules resulting from heme catabolism by HO-1. Particularly, carbon monoxide (CO) has been implicated as an immunomodulatory second messenger able to prime macrophages for increased bacterial killing via indirect NLRP3 inflammasome activation[43]. This opens the possibility that CO could help reduce the deleterious effects of excess heme on host resistance.

Our finding that DOCK8 is necessary for the cytoskeleton changes and disruption of bacterial phagocytosis by heme is in line with recent studies showing that DOCK8 regulates dendritic cell migration via Cdc42[37, 44]. We speculate that heme stimulates DOCK8 GEF activity, either directly or indirectly via a DOCK8-containing protein complex. While it is unlikely that this association is relevant under homeostasis, exhaustion of heme-scavenging proteins following

severe hemolysis[7, 8] might render it especially significant for bacterial infections. As such, *Dock8*$^{-/-}$>WT chimeric mice were protected from elevated heme during sepsis. However, the improved bacterial clearance in the absence of DOCK8 was incomplete, and likely represents a tradeoff between beneficial effects of DOCK8 deletion upon hemolysis, and inevitable immune defects caused by DOCK8 deficiency[37, 45]. Nevertheless, the net gain in resistance against bacteria further reinforces the relevance of this mechanism during bacterial sepsis. DOCK8 is an intracellular protein thought to be anchored to the cell membrane where it controls cell movement and shape[46]. Thus, understanding precisely how heme gains access to the cytoplasm of innate immune cells could prove useful for therapeutic strategy developments, and might be attainable by complexing extracellular heme or by targeting heme transporters to prevent heme internalization.

The effects of excess heme on host resistance identified by us seem surprising considering the weight malaria has had in shaping the human genome. However, it is important to recognize that these events occur mainly following systemic inflammation or in people with homozygous sickle hemoglobin, where even highly conserved mechanisms to scavenge and degrade heme are overwhelmed[9]. It is reasonable to speculate that the need to mitigate the impact of excess heme on vital organs is such that it takes priority over host defense mechanisms, especially given the fact that both functions are essentially coordinated by macrophages.

Rising antibiotic resistance and widespread prophylactic antibiotic use created an urgent need for novel therapeutic strategies. As a proof-of-concept, our findings demonstrate that quinine treatment is able to prevent cytoskeletal changes and phagocytosis inhibition induced by heme. Quinine is a long-standing antimalarial drug, whose mechanism of action is not fully understood, although it has been reported that quinine forms complexes with heme[47], indicating that quinine might interfere with the association of heme with DOCK8 through steric hindrance. This is important since targeting heme effects upstream of Cdc42 signaling should conserve its normal function. Our results with quinine suggest that adjuvant immunotherapy strategies focused on restoring host resistance are a viable alternative in fighting the increased infection rates resulting from hemolysis.

Taken together, our findings uncover an unexpected effect of heme on the innate immune response and pave the way towards future therapeutic approaches. This could have far-reaching

implications not only for patients with inherited hemolytic disorders, but importantly, also for patients with acquired hemolysis, as seen in malaria, systemic inflammation and sepsis.

Acknowledgements

Y. Fukui (Medical Institute of Bioregulation, Kyushu University, Japan) and J. Stein (Theodor Kocher Institute, University of Bern, Switzerland) are acknowledged for providing the DOCK8 deficient bone marrow and H. Häcker (St. Judes Childrens Research Hospital, Tennessee, USA) for providing the ERHBD-HoxB8 encoding retroviral construct. pSpCas9(BB)-2a-Puro (PX459) was a gift from F. Zhang (Addgene plasmid # 48139); pGRG36 was a gift from N. Craig (Addgene plasmid # 16666). LifeAct-GFP encoding retrovirus was kindly provided by A. Leithner (Institute of Science and Technology Austria, Klosterneuburg, Austria). pSIM8 and TKC *E. coli* were gifts from D. L. Court (Center for Cancer Research, National Cancer Institute, Frederick MD, USA). We acknowledge M. Gröger and S. Rauscher for excellent technical support (Core imaging facility, Medical University of Vienna, Vienna, Austria). We thank D. P. Barlow and L. R.Cheever for critical reading of the manuscript. This work was supported by the Austrian Academy of Sciences, the Science Fund of the Austrian National Bank (14107) and the Austrian Science Fund FWF (I1620-B22) within the Infect-ERA framework (to S.K).

Author Contributions

R.M. performed and designed *in vivo*, *in vitro*, pull-down and confocal microscopy experiments, analyzed data, performed bioinformatics analysis. K.V.M.H. performed pull-down experiments. J.M. assisted with *in vitro* and *in vivo* experiments. A.D.G. assisted with CRISPR/Cas9 KO clone generation. O.S. performed efferocytosis assay. P.S., S.S., F.Q., R.G., K.L., A.H., A.K., B.R.-S., and M.D. provided experimental support. T.D. designed and M.C.A. performed *L. monocytogenes* experiments. M.B. performed Cellix experiments. D.K., H.E. and S.C.E. provided reagents or mice. J.C. and K.B. analyzed LCMS experiments. M.S. and G.S.F. provided technical and intellectual support. S.K. designed and supervised the research. R.M. and S.K. wrote the manuscript. All authors reviewed the manuscript.

Competing financial interests

The authors declare no competing financial interests.

References

1. Modell, B. & Darlison, M. Global epidemiology of haemoglobin disorders and derived service indicators. *Bulletin of the World Health Organization* **86**, 480-487 (2008).

2. World Health Organization. *World malaria report 2013*. World Health Organization: Geneva, 2013.

3. Adamzik, M. *et al.* Free hemoglobin concentration in severe sepsis: methods of measurement and prediction of outcome. *Crit Care* **16**, R125 (2012).

4. Larsen, R. *et al.* A central role for free heme in the pathogenesis of severe sepsis. *Sci Transl Med* **2**, 51ra71 (2010).

5. Schaer, D.J., Buehler, P.W., Alayash, A.I., Belcher, J.D. & Vercellotti, G.M. Hemolysis and free hemoglobin revisited: exploring hemoglobin and hemin scavengers as a novel class of therapeutic proteins. *Blood* **121**, 1276-1284 (2013).

6. Muller-Eberhard, U., Javid, J., Liem, H.H., Hanstein, A. & Hanna, M. Plasma concentrations of hemopexin, haptoglobin and heme in patients with various hemolytic diseases. *Blood* **32**, 811-815 (1968).

7. Dutra, F.F. & Bozza, M.T. Heme on innate immunity and inflammation. *Front Pharmacol* **5**, 115 (2014).

8. Smith, A. & McCulloh, R.J. Hemopexin and haptoglobin: allies against heme toxicity from hemoglobin not contenders. *Front Physiol* **6**, 187 (2015).

9. Gozzelino, R., Jeney, V. & Soares, M.P. Mechanisms of cell protection by heme oxygenase-1. *Annual review of pharmacology and toxicology* **50**, 323-354 (2010).

10. Chiabrando, D., Vinchi, F., Fiorito, V., Mercurio, S. & Tolosano, E. Heme in pathophysiology: a matter of scavenging, metabolism and trafficking across cell membranes. *Front Pharmacol* **5**, 61 (2014).

11. Fortes, G.B. *et al.* Heme induces programmed necrosis on macrophages through autocrine TNF and ROS production. *Blood* **119**, 2368-2375 (2012).

12. Seixas, E. *et al.* Heme oxygenase-1 affords protection against noncerebral forms of severe malaria. *Proc Natl Acad Sci U S A* **106**, 15837-15842 (2009).

13. Ramakrishnan, M. *et al.* Increased risk of invasive bacterial infections in African people with sickle-cell disease: a systematic review and meta-analysis. *The Lancet. Infectious diseases* **10**, 329-337 (2010).

14. Wiener, E. Impaired phagocyte antibacterial effector functions in beta-thalassemia: a likely factor in the increased susceptibility to bacterial infections. *Hematology* **8**, 35-40 (2003).

15. Church, J. & Maitland, K. Invasive bacterial co-infection in African children with Plasmodium falciparum malaria: a systematic review. *BMC medicine* **12**, 31 (2014).

16. Scott, J.A. *et al.* Relation between falciparum malaria and bacteraemia in Kenyan children: a population-based, case-control study and a longitudinal study. *Lancet* **378**, 1316-1323 (2011).

17. Cober, M.P. & Phelps, S.J. Penicillin prophylaxis in children with sickle cell disease. *The journal of pediatric pharmacology and therapeutics : JPPT : the official journal of PPAG* **15**, 152-159 (2010).

18. Hirst, C. & Owusu-Ofori, S. Prophylactic antibiotics for preventing pneumococcal infection in children with sickle cell disease. *The Cochrane database of systematic reviews* **11**, CD003427 (2014).

19. Dutra, F.F. *et al.* Hemolysis-induced lethality involves inflammasome activation by heme. *Proc Natl Acad Sci U S A* **111**, E4110-4118 (2014).

20. Cassat, J.E. & Skaar, E.P. Iron in infection and immunity. *Cell host & microbe* **13**, 509-519 (2013).

21. Cunnington, A.J. *et al.* Prolonged neutrophil dysfunction after Plasmodium falciparum malaria is related to hemolysis and heme oxygenase-1 induction. *J Immunol* **189**, 5336-5346 (2012).

22. Cunnington, A.J., de Souza, J.B., Walther, M. & Riley, E.M. Malaria impairs resistance to Salmonella through heme- and heme oxygenase-dependent dysfunctional granulocyte mobilization. *Nat Med* **18**, 120-127 (2012).

23. Ganz, T. Macrophages and systemic iron homeostasis. *Journal of innate immunity* **4**, 446-453 (2012).

24. Jais, A. *et al.* Heme oxygenase-1 drives metaflammation and insulin resistance in mouse and man. *Cell* **158**, 25-40 (2014).

25. Skaar, E.P. The battle for iron between bacterial pathogens and their vertebrate hosts. *PLoS Pathog* **6**, e1000949 (2010).

26. Wandersman, C. & Stojiljkovic, I. Bacterial heme sources: the role of heme, hemoprotein receptors and hemophores. *Curr Opin Microbiol* **3**, 215-220 (2000).

27. Letoffe, S., Delepelaire, P. & Wandersman, C. The housekeeping dipeptide permease is the Escherichia coli heme transporter and functions with two optional peptide binding proteins. *Proc Natl Acad Sci U S A* **103**, 12891-12896 (2006).

28. Flannagan, R.S., Jaumouille, V. & Grinstein, S. The cell biology of phagocytosis. *Annual review of pathology* **7**, 61-98 (2012).

29. Moulding, D.A., Record, J., Malinova, D. & Thrasher, A.J. Actin cytoskeletal defects in immunodeficiency. *Immunol Rev* **256**, 282-299 (2013).

30. McEver, R.P. & Zhu, C. Rolling cell adhesion. *Annual review of cell and developmental biology* **26**, 363-396 (2010).

31. Wagener, F.A. *et al.* Different faces of the heme-heme oxygenase system in inflammation. *Pharmacol Rev* **55**, 551-571 (2003).

32. Choi, H. *et al.* SAINT: probabilistic scoring of affinity purification-mass spectrometry data. *Nat Methods* **8**, 70-73 (2011).

33. Mellacheruvu, D. *et al.* The CRAPome: a contaminant repository for affinity purification-mass spectrometry data. *Nat Methods* **10**, 730-736 (2013).

34. Franceschini, A. *et al.* STRING v9.1: protein-protein interaction networks, with increased coverage and integration. *Nucleic acids research* **41**, D808-815 (2013).

35. Ridley, A.J. Life at the leading edge. *Cell* **145**, 1012-1022 (2011).

36. Heasman, S.J. & Ridley, A.J. Mammalian Rho GTPases: new insights into their functions from in vivo studies. *Nat Rev Mol Cell Biol* **9**, 690-701 (2008).

37. Harada, Y. *et al.* DOCK8 is a Cdc42 activator critical for interstitial dendritic cell migration during immune responses. *Blood* **119**, 4451-4461 (2012).

38. Lee, D.J., Cox, D., Li, J. & Greenberg, S. Rac1 and Cdc42 are required for phagocytosis, but not NF-kappaB-dependent gene expression, in macrophages challenged with Pseudomonas aeruginosa. *J Biol Chem* **275**, 141-146 (2000).

39. Hill, G.B. Enhancement of experimental anaerobic infections by blood, hemoglobin, and hemostatic agents. *Infection and immunity* **19**, 443-449 (1978).

40. Nairz, M., Haschka, D., Demetz, E. & Weiss, G. Iron at the interface of immunity and infection. *Front Pharmacol* **5**, 152 (2014).

41. Flannagan, R.S., Cosio, G. & Grinstein, S. Antimicrobial mechanisms of phagocytes and bacterial evasion strategies. *Nature reviews. Microbiology* **7**, 355-366 (2009).

42. Sarantis, H. & Grinstein, S. Subversion of phagocytosis for pathogen survival. *Cell host & microbe* **12**, 419-431 (2012).

43. Wegiel, B. *et al.* Macrophages sense and kill bacteria through carbon monoxide-dependent inflammasome activation. *J Clin Invest* **124**, 4926-4940 (2014).

44. Krishnaswamy, J.K. *et al.* Coincidental loss of DOCK8 function in NLRP10-deficient and C3H/HeJ mice results in defective dendritic cell migration. *Proc Natl Acad Sci U S A* **112**, 3056-3061 (2015).

45. Zhang, Q. *et al.* Combined immunodeficiency associated with DOCK8 mutations. *N Engl J Med* **361**, 2046-2055 (2009).

46. Nishikimi, A., Kukimoto-Niino, M., Yokoyama, S. & Fukui, Y. Immune regulatory functions of DOCK family proteins in health and disease. *Exp Cell Res* **319**, 2343-2349 (2013).

47. Leed, A. *et al.* Solution structures of antimalarial drug-heme complexes. *Biochemistry* **41**, 10245-10255 (2002).

Figure legends

Figure 1. **Heme impairs bacterial clearance *in vivo*.**

(**a**) Pearson's correlation between heme levels and bacterial burden in WT mice 16h post-infection with *E. coli* (n=30). (**b, c**) Naïve WT mice (n=8) or WT mice pretreated with PBS (n=8) or heme (n=8) and respective heme plasma amounts (**b**) and bacterial counts (**c**) 16h post-infection with *E. coli*. (**d**) Survival of WT mice pretreated with PBS (n=12) or heme (n=12) and infected with *E. coli*. (**e, f**) Plasma heme levels (**e**) of naïve WT (n=8) or infected *LysM*-Cre$^{-/-}$*Hmox1*$^{fl/fl}$ (n=7) and *LysM*-Cre$^{+/-}$*Hmox1*$^{fl/fl}$ (n=8) mice and respective bacterial counts (**f**) 16h post-infection with *E. coli*. (**g**) Survival of *LysM*-Cre$^{-/-}$*Hmox1*$^{fl/fl}$ (n=15) and *LysM*-Cre$^{+/-}$*Hmox1*$^{fl/fl}$ (n=11) mice infected with *E. coli*. Data in (**a**) are pooled from 3 independent experiments. Data in (**b-f**) are representative of 2 independent experiments. Data in (**b**, **c**, **e**, **f**) is presented as mean, and dots represent individual animals. (**b**, **e**) one-way ANOVA with Tukey's multiple comparison test, (**c**, **f**) Mann-Whitney test, (**d, g**) Mantel-Cox test; * $p \leq 0.05$, ** $p \leq 0.01$, *** $p \leq 0.001$, **** $p \leq 0.0001$.

Figure 2. Increased bacterial burden triggered by heme is independent of heme-iron acquisition.

(**a**) Mid-log phase difference in the growth of *E. coli* in LB medium or in iron-chelated LB medium (deferoxamine, +DFO), supplemented with DMSO (control) or heme (3, 10 and 30μM). Data are presented as the $\log_{10}$ difference (normalized to control) in viable colony forming units (CFU) 4.5 h (mid-log phase) post-inoculation of media (n=3 per condition). (**b, c**) Plasma heme levels (**b**) of naïve WT mice (n=8) or WT mice pretreated with PBS (n=8) or heme (n=6) and respective bacterial counts (**c**) 16h after infection with Δ*dppC::kan*^{R} *E. coli*. (**d-f**) Plasma heme levels (**d**) of naïve WT mice (n=8) or WT mice pretreated with PBS (n=8), heme (n=7), or an equimolar amount of free ferric iron (n=8; ferric ammonium citrate) and respective total liver iron levels (**e**), and bacterial counts (**f**) 16h post-infection with *E. coli*. (**g, h**) Plasma heme levels (**g**) of naïve WT mice (n=8) or WT mice infected with isogenic non-hemolytic (n=8; *E. coli*) and hemolytic (n=8; *E. coli* $^{hlyABCD::attTn7}$) *E. coli* strains and respective bacterial counts (**h**) 16h post-infection. Floating bars in (**a**) are presented as the mean ± min. and max. values. Data in (**b-h**) is presented as mean, and dots represent individual animals. (**a**, **b**, **d-g**) one-way ANOVA with

590 Tukey's multiple comparison test, (**c**, **h**) Mann-Whitney test; n.s. = not significant, * $p \leq 0.05$,
591 ** $p \leq 0.01$, *** $p \leq 0.001$, **** $p \leq 0.0001$.

592 **Figure 3. Heme potently inhibits phagocytosis of bacteria.**

593 (**a**) Phagocytosis of FITC-*E. coli* by RAW264.7 macrophages treated with control (DMSO) or
594 heme (n=4 per condition) and assessed by flow cytometry. (**b**) Confocal microscopy images of
595 RAW264.7 macrophages treated with control (DMSO) or heme and incubated with FITC-*E. coli*.
596 (automatic quantification in Supplementary Fig. 3a). Scale bar = 20 μm. (**c-f**) Phagocytosis of
597 FITC-*E. coli* by primary mouse peritoneal macrophages (**c**), mouse neutrophils (**d**), human
598 monocyte-derived macrophages (**e**), and human neutrophils (**f**), treated with control (DMSO) or
599 heme (n=4 per condition) and quantified by flow cytometry. (**g**) Phagocytosis of bacteria by
600 human blood neutrophils ($CD11b^+$, SSC^{high}) and monocytes ($CD11b^+$, SSC^{low}) from control and
601 heme-treated whole blood (n=4 per condition) as quantified by flow cytometry. (**h**) Time course
602 of phagocytosis of FITC-*E. coli* by RAW264.7 macrophages treated with control (DMSO), heme
603 or heme treatment and subsequent washing to remove heme prior to incubation with bacteria
604 (n=4 per condition and time point; flow cytometry analysis). (**i**) Percentage of cell death,
605 (measured by LDH release; left panel), and cell viability, (measured by neutral red assay; right
606 panel), of RAW264.7 macrophages upon incubation with control (DMSO) or heme (n=4 per
607 condition and time point). Staurosporine treatment (10μM) was used as a positive control to
608 determine the max. cell death and loss of viability for LDH release assays and neutral red assays,
609 respectively. (**j**) *In vivo* phagocytosis of FITC-*E. coli* by peritoneal macrophages (%$FITC^+$
610 $F4/80^+$, $CD11b^+$, $Ly6G^-$) from PBS- or heme-treated mice (n=5 per condition), shown and
611 quantified by flow cytometry. Percentage of $FITC^+$ B-cells ($CD11b^-$, $CD3^-$, $B220^+$, $Ly6G^-$,
612 $F4/80^-$) shown as control for unspecific binding of bacteria to cells. (**k**) Giemsa stain of cells
613 from peritoneal exudates of mice treated with PBS or heme 16h post-infection with *E. coli* as in
614 Fig. 1c and 1d. Bacteria are stained blue and scale bar = 5 μm. Data in (**a**) are representative of 4
615 independent experiments. Data in (**b**, **d**, **e**, **g, i-k**) are representative of 2 independent
616 experiments. Data in (**a**, **c-j**) is presented as mean ± S.E.M.. (**a**, **d-g**) one-way ANOVA with
617 Tukey's multiple comparison test, (**c** and **j**) two-tailed t-test, (**h**, **i**) two-way ANOVA with
618 Tukey's multiple comparison test; * $p \leq 0.05$, ** $p \leq 0.01$, *** $p \leq 0.001$, **** $p \leq 0.0001$.
619

620 **Figure 4. Heme induces cell shape changes via actin cytoskeleton remodeling.**

(**a, b**) Cellular morphology of RAW264.7 macrophages (**a**) and human monocyte-derived macrophages (**b**) incubated with control (DMSO) or heme for 15min. Scale bar = 20 μm. (**c**) Live cell imaging of RAW264.7 macrophages expressing LifeAct-GFP treated with control (DMSO) or 3μM heme (see **Supplementary Video 2**). Scale bar = 10 μm. (**d, e**) Cell shape analysis and automatic quantification of cell area and form factor of RAW264.7 macrophages (**d**) (n=177-282 cells analyzed per condition) and human monocyte-derived macrophages (**e**) (n= 6 images per condition) incubated with control (DMSO) or heme for 15min. Scale bar = 20 μm. Data in (**a** and **d**) are representative of 6 independent experiments. Data in (**c**) are representative of 2 independent experiments. Data in (**d**, **e**) are presented as mean ± S.E.M.; (**d**, **e**) one-way ANOVA with Tukey's multiple comparison test; * $p \leq 0.05$, *** $p \leq 0.001$, **** $p \leq 0.0001$.

Figure 5. Heme interferes with actin cytoskeleton-dependent functions

(**a, b**) Migration of BMDM treated with control (DMSO) or heme, as measured by wound closure (scratch) assay (n=5 per condition and time point). Scale bar = 200 μm. (**c, d**) Dendritic cell migration in a 3D collagen matrix in response to a CCL19 chemokine gradient. Data in (**c**) represent the tracks and corresponding distances (px) for 100 randomly selected tracks for each condition (upper panels). Lower panels represent track directionality and are presented as a wind rose plot of the number of tracks within a 33° angle from the center of each bin (36 bins, 10° each). Data in (**d**) are presented as the nonlinear regression for each condition plus the mean – S.E.M. for each measurement in each condition. Data in (**a**, **b**) are representative of 2 independent experiments. Data in (**c**, **d**) are pooled from 3 independent experiments. Data in (**b**) are presented as mean ± S.E.M.; (**b**) two-way ANOVA with Tukey's multiple comparison test **** $p \leq 0.0001$.

Figure 6. Identification of the mechanism of heme-induced cytoskeletal interference.

(**a**) Competition analysis and results of computational analyses using the SAINT and CRAPome database bioinformatics tools (n=2 replicates per experiment). (**b**) STRING database network analysis of heme associated proteins from (**a**) that are involved in actin cytoskeleton remodeling. Edge thickness represents interaction confidence as reported by the STRING database v9.1. Solid edges = interactions reported for mouse, dashed edges = human ortholog projections. (**c**) Western blot validation of heme associated proteins. E.B. = empty beads; H.B. = heme beads; H.B.C. =

heme beads, heme-competed sample. (**d**) Cdc42 G-LISA assay measuring the activation of Cdc42 in RAW264.7 macrophages treated with PBS or heme (n=3 per condition and time point). (**e, f**) Representative images of cellular morphology (**e**) of RAW264.7 macrophages pretreated with control (DMSO), ML141 (CDC42 inhibitor) or ML141 treatment and subsequent washing to remove ML141, and treated with control (DMSO) or heme for 15min, and automatic quantification of form factor (**f**) (n=4 random fields per condition; see automatic quantification of cell area in Supplementary Fig. 7b). (**g**, **h**) Cellular morphology (**g**) of RAW264.7 macrophages pretreated with control (DMSO) or K216-0381 (mDIA2 inhibitor), and treated with control (DMSO) or heme for 15min, and corresponding automatic quantification of form factor (**h**) (n=4 random fields per condition). Data in (**a** and **b**) are based on 2 independent experiments for each condition. Data in (**c**-**f**) are representative of 2 independent experiments. Data in (**d**, **f, h**) are presented as mean ± S.E.M.. (**d**) two-way ANOVA with Tukey's multiple comparison test, (**f, g**) one-way ANOVA with Tukey's multiple comparison test; n.s. = not significant, * $p \leq 0.05$, ** $p \leq 0.01$, *** $p \leq 0.001$, **** $p \leq 0.0001$. Scale bars = 20 μm.

Figure 7. DOCK8 mediates heme-induced actin cytoskeleton changes and suppression of phagocytosis.

(**a, b**) Cellular morphology of WT and *Dock8*$^{-/-}$ HoxB8 macrophages (**a**) treated with control (DMSO) or heme for 15min and (**b**) corresponding automatic quantification of form factor (n=4-8 images per condition). Scale bars = 20 μm. (**c**) Cdc42 G-LISA assay measuring the activation of Cdc42 in WT and *Dock8*$^{-/-}$ HoxB8 macrophages treated with PBS or heme (10μM) for 10min (n=3 per condition). (**d**) Phagocytosis of FITC-*E. coli* by WT and *Dock8*$^{-/-}$ BMDM pretreated with control (DMSO) or heme (n=4 per condition), analyzed by flow cytometry. (**e, f**) Plasma heme levels (**e**) of naïve WT mice (n=8) or WT>WT and *Dock8*$^{-/-}$>WT bone marrow chimeras pretreated with PBS (n=7-8) or heme (n=7) and respective bacterial counts (**f**) 16h after infection with *E. coli*. Data in (**a**, **b**, **d**) are representative of 2 independent experiments. Data in (**b**-**d**) are presented as mean ± S.E.M. and data in (**e**, **f**) is presented as mean, and dots represent individual animals; (**b**-**f**) one-way ANOVA with Tukey's multiple comparison test, n.s. = not significant, * $p \leq 0.05$, ** $p \leq 0.01$, **** $p \leq 0.0001$.

Figure 8. Quinine restores phagocytosis of bacteria *in vitro* and *in vivo*.

(a) Effect of compounds on phagocytosis of bacteria by RAW264.7 macrophages. Data are presented as the $\log_2$ fold change in phagocytosis induced by each compound vs. DMSO control (x-axis) or vs. heme (y-axis). Bubble size and color represent the compound scores derived from the median and mean phagocytosis values, respectively. **(b, c)** Phagocytosis of FITC-*E. coli* by RAW264.7 macrophages (**b**) and human monocyte-derived macrophages (n=3) (**c**) pretreated with control (saline) or quinine, and treated with control (DMSO) or heme as assessed by flow cytometry. **(d)** Western blot assessment of the influence of quinine on the association of DOCK8, LGALS3 or MPP1 to heme. E.B. = empty beads; H.B. = heme beads; H.B.C. = heme beads, heme-competed sample, H.B.Qui. = heme beads, quinine-competed sample. **(e)** *In vivo* phagocytosis of heat-killed FITC-*E. coli* by peritoneal macrophages ($F4/80^+$, $CD11b^+$, $Ly6G^-$) from mice pretreated with mock (PBS) or quinine, and treated with PBS or heme (n=4 per condition), and quantified as the percentage of $FITC^+$ macrophages by flow cytometry (left panel shows representative plots). **(f)** Plasma heme levels of naïve WT mice (n=8) or WT mice pretreated with mock (PBS) or 60mg/kg quinine, and treated with PBS or heme, and **(g)** respective bacterial counts 16h post-infection with *E. coli* (n=7 per group of infected mice). **(h)** Survival of WT mice pretreated with mock (PBS) or quinine, and treated with PBS or heme (n=11-12 per group, quinine and heme dose as in **f** and **g**). Data in **(b, d, f** and **g)** are representative of 2 independent experiments. Data in **(b, c, e)** are presented as mean ± S.E.M. Data in **(f, g)** is presented as mean, and dots represent individual animals; (**a**) C-score analysis – see methods section, (**b, c, e-g**) one-way ANOVA with Tukey's multiple comparison test, (**h**) Mantel-Cox test; n.s. = not significant, * $p \leq 0.05$, ** $p \leq 0.01$, *** $p \leq 0.001$, **** $p \leq 0.0001$.

Online Methods

Mice

Sex- and age-matched 8-10 week old WT C57BL/6, LysMCre$^{-/-}$*Hmox1*$^{fl/fl}$ and littermate LysMCre$^{+/-}$*Hmox1*$^{fl/fl}$ mice were used. All mice were kept in SPF conditions, with 12h light/dark cycle, unrestricted access to food and water, and environmental enrichment. For bone marrow transplant and bone marrow macrophage generation experiments, healthy female WT C57BL/6 and *Dock8*$^{-/-}$ mice were used[44]. All *in vivo* experiments were performed in accordance with Austrian law and after approval by the Institutional Review Board of the Medical University of Vienna and the Austrian Ministry of Sciences (BMWF-66.009/0277-II/3b/2013).

Reagents and ELISA

Heme (hemin), hemoglobin, quinine (quinine hydrochloride dihydrate), 2,2'-bipyridyl, Ammonium iron (III) citrate, Iron (II) sulfate, neutral red, CK666, ML-141, *E. coli* O55:B5 LPS, phenylhydrazine, *N*-acetyl-*L*-cysteine, trichloroacetic acid, bathophenanthroline disulfonic acid, ascorbic acid, staurosporine, estradiol, bradykinin, DAPI, phalloidin-TRITC, Hoechst 33258 and hemin-agarose were from Sigma. PPIX (protoporphyrin IX, Frontier Scientific), SnPPIX (tin protoporphyrin IX, Santa Cruz Biotechnology), deferoxamine (Desferal®, Novartis), DMSO (CryoSure DMSO, WAK – Chemie Medical GmbH), K216-0385[54] (ChemDiv), cytochalasin D (Calbiochem), phalloidin-Alexa Fluor 633 and CellMask™ Orange (Life Technologies™), rhM-CSF, and IL-3 (PeproTech), GM-CSF and IL-6 (eBioscience), TMB substrate (Thermo Scientific)

For flow cytometry Ly-6G-PE or PE/Cy7 (clone 1A8), CD11c-APC or PerCP/Cy5.5 (N418), F4/80-PE/Cy7 or FITC (BM8), CD45.1-APC (A20), CD45.2-PerCP/Cy5.5 (104), CD11b Pacific blue (M1/70), CD19-Brilliant Violet 605 or PE (6D5), and Ly-6C-Brilliant Violet 605 (HK 1.4) were from BioLegend. CD3-APC (17A2), B220-PerCP-Cy5.5 (RA3-6B2), CD11b-Alexa Fluor 700 (M1/70), Fixable Viability Dye eFluor® 780 were from eBioscience. CD3e-V500 (500A2), CD11c-FITC (HL3), CD45-V500 (30-F11) were from BD biosciences. ELISA kits for mouse KC, MCP-1, TNF and IL-6 were from R&D Systems. Rabbit polyclonals against DOCK8 (#11622-1-AP), MPP1 (#14715-1-AP), ARPC3 (#14652-1-AP), ATP6V1A (#17115-1-AP), and

735 Galectin-3 (LGALS3) (#14979-1-AP) were from Proteintech. Anti-beta-actin antibody (AC-15,
736 Sigma), anti Cdc42 (4B3, Cytoskeleton Inc.); goat anti-rabbit IgG, HRP-linked antibody (#7074,
737 Cell Signaling) and goat anti-mouse IgG (H+L), HRP-linked antibody (#170-6516, Bio-Rad)
738 were used. All flow cytometry analysis was done using FlowJo (v10).

739

740 **Cell isolation, stimulation and culture**

741 Peritoneal macrophages were obtained from the peritoneal lavage fluid of WT mice, resuspended
742 in RPMI-1640 supplemented with 10% FCS and penicillin/streptomycin (pen/strep). Bone
743 marrow cells were collected from tibia and femur of WT and *Dock8*$^{-/-}$ mice and differentiated in
744 RPMI-1640 with 10% FCS, pen/strep and 10% L929 conditioned medium for 7 days to generate
745 BMDMs, or GM-CSF (20ng/ml) for 8 days and 24h with *E. coli* LPS (200ng/ml) to generate
746 BMDC. DOCK8 deficient precursor cell line and control cell lines were generated by HoxB8
747 induced conditional immortalization as previously described[55]. Briefly, bone marrow of *Dock8*$^{-/-}$
748 and WT mice was suspended in RPMI-1640 with 10ng/ml IL-3, 20ng/ml IL-6 and 1%
749 supernatant of an SCF producing cell line for two days, followed by 5% FLT3 supernatant and
750 1µM estradiol and spin infected with retrovirus encoding estrogen inducible ERHBD-HoxB8[55].
751 Mouse neutrophils were collected from peritoneal exudates of mice 4 h after thioglycollate
752 treatment, purity >90% was confirmed by Giemsa-stained cytospins. RAW264.7 macrophages
753 (ATCC TIB-71®) were maintained in RPMI-1640 with 10% FCS and pen/strep.

754 Human neutrophils and monocytes were isolated from peripheral blood from healthy donors
755 (after obtaining informed consent from all donors) via OptiPrep™ density gradient centrifugation
756 (Axis-Shield). Human monocytes were differentiated into human monocyte-derived macrophages
757 (hMDM) in RPMI-1640,10% FCS, pen/strep and rhM-CSF (10ng/ml) for 7 days. BMDM, PM,
758 hMDM or RAW264.7 macrophages were allowed to adhere for 3 h before stimulation. Heme
759 (hemin) and PPIX stocks for *in vitro* studies were prepared to 10mM in DMSO, stored at -20°C
760 and used within 3 months. SnPPIX and hemoglobin stocks were prepared to 5mM in PBS. All
761 porphyrin and hemoglobin stimulations were done 15min prior to the assay, unless otherwise
762 indicated. Cell lines were routinely checked for *mycoplasma* contamination.

763

764

765

766 **Bone marrow transplant**

767 Bone marrow chimeras were generated as described before[56]. Briefly, 8-week-old WT recipient
768 mice were lethally irradiated and $5x10^5$ bone marrow cells from WT or *Dock8*$^{-/-}$ mice were
769 retroorbitally injected. 6 weeks later successful engraftment was verified using flow cytometry
770 using the following gating strategy: neutrophils: CD11b$^+$, Ly6G$^+$; T-cells: CD11b$^-$, CD3$^+$,
771 CD19$^-$; B-cells: CD11b$^-$, CD3$^-$, CD19$^+$; monocytes: CD11b$^+$, Ly6G$^-$; macrophages: CD3$^-$,
772 CD19$^-$, F4/80$^+$; DCs: CD3$^-$, CD19$^-$, F4/80$^-$, CD11c$^+$. Distinction between donor and recipient
773 cells was assessed by CD45.1 or CD45.2 variant expression.

774

775 ***E. coli* and sterile peritonitis models**

776 Murine peritonitis was induced as previously described[56]. Briefly, *E. coli* (strain PMV-1, serotype
777 O18:K1) or its isogenic mutants (**Supplementary Table 1**) were cultured in Luria-Bertani
778 medium and mice were infected via intraperitoneal (i.p.) injection with ~$1x10^4$ CFU in 200µl.
779 Where indicated, mice received 100µL i.p. of PBS, heme (25 µmol/kg body weight) or
780 ammonium iron (III) citrate (25 µmol iron/kg body weight) 30min prior to infection with *E. coli*.
781 Heme stock solutions for *in vivo* administration were prepared by dissolving hemin to 5mM in
782 0.2M NaOH, pH 7.5 and stored at -80°C. Quinine-treated mice were given one dose (6h end
783 point) or two doses (16h end point) 1h before and 6h after infection, respectively (60mg/kg each
784 dose). Serial dilutions of tissue samples were plated to enumerate viable bacteria. In survival
785 studies mortality was monitored every 1 to 2h. LPS endotoxemia was induced by i.p. injection of
786 *E. coli* LPS (40mg/kg). For thioglycollate peritonitis, mice were pretreated PBS or heme as
787 described above prior to injection of 1ml 4% thioglycollate broth[57]. Blood and peritoneal lavage
788 fluid were collected 6h post-injection and cell influx into the peritoneal cavity was assessed on
789 cytospin preparations stained with Giemsa, and via flow cytometry (LSRFortessa). Cells were
790 gated on viable CD45$^+$ cells and further gated as: neutrophils: Ly6G$^+$ CD11b$^+$, F4/80$^-$, CD3$^-$,
791 CD19$^-$, and macrophages: F4/80$^+$, CD11b$^+$, Ly-6G$^-$, CD3$^-$, CD19$^-$.

792

793 ***L. monocytogenes* infection model**

Mice were infected by intraperitoneal injection of $1x10^6$ CFU genetically optimized *L. monocytogenes* strain LO28InlA*[58]. The bacteria were prepared as previously described[59]. For detection of bacterial loads (CFU assays), mice were sacrificed at the indicated time points, spleens were homogenized and plated on Oxford agar plates for 24h at 37 °C.

Heme and total liver iron measurements

Plasma levels of heme were measured using its pseudoperoxidase activity as described earlier[60]. Briefly, standard dilutions and samples were diluted in PBS 1% BSA, incubated with TMB substrate and absorbance was measured at 450nm. Additionally, concentration of standard dilutions was confirmed using the heme-chromogen method[61], and calculated using Beer's law[61].

Total liver iron levels were measured as previously described[62], with the following modifications to detect total iron levels. Briefly, 100µl (=20mg tissue) of liver homogenate were hydrolyzed at 65°C with 50µl TCA-HCl solution (16h), and boiled 1h at 120°C to release heme. Clarified samples were incubated with sodium acetate, bathophenanthroline disulfonic acid and ascorbic acid solution for 5min at RT, absorbance was measured at 540nm and iron concentration was calculated using $[Fe] = (((A_s - A_b) \times V \times MW))/((e \times l \times t))$, ($A_s$: sample absorbance, A_b: blank absorbance, V: volume, MW: molecular weight of iron, e: milimolar absorptivity of bathophenanthroline disulfonic acid, l: path length and t: weight of tissue). Measured concentrations were verified against standard samples with known iron concentrations.

Cloning and bacteria

The *E. coli* dppC gene was deleted using a recombineering approach as described previously[49]. λ-RED plasmid pSIM8 was electroporated into *E. coli* (PMV-1) and the kanamycin resistance gene was PCR-amplified from *E. coli* TKC with the primer set DppC_Kan_For-DppC_Kan_Rev, with 45bp homology arms flanking the dppC gene. Amplicon was electroporated into induced PMV-1-pSIM8 *E. coli*. Correct substitution of dppC by nptII was verified by PCR using the primer set DppC_R1-_For-DppC_R1-_Rev. pSIM8 plasmid was cured and functional dppC deletion was verified by loss of heme-iron utilization (**Supplementary Fig. 1j**) generating Δ*dppC::Kan*^{R} *E. coli*. The hemolysin operon from *E. coli* CFT073, including its upstream regulatory elements[63], was PCR-amplified using primer set Hly_NotI_For-Hly_XhoI_Rev,

824 double-digested with NotI-HF and XhoI and ligated to mini-Tn7 plasmid pGRG36[52] to generate
825 pRM24. pRM24 was electroporated into PMV-1 *E. coli*. Insertion of the hemolysin operon onto
826 the *E. coli* attTn7 site was confirmed using the primer sets attTn7_Left_For-attTn7_Left_Rev and
827 attTn7_Right_For-attTn7_Righ_Rev. the plasmid was cured to generate *E. coli* $^{hlyABCD::attTn7}$. See
828 **Supplementary Tables 1-3**.

829

830 **CRISPR-Cas9 mediated gene deletion**

831 Mouse *Mpp1* and *Lgals3* genes were deleted in RAW264.7 macrophages using CRISPR-Cas9
832 system[53]. Briefly, Cas9 and sgRNA expressing plasmids were generated by digesting the
833 pSpCas9(BB)-2A-Puro (pX459) vector[53] with BbsI (New England Labs). Unphosphorylated
834 oligos targeting exon 1 of *Mpp1*, (oligo pair *Mpp1*_del_For-*Mpp1*_del_Rev) or exon 2 of *Lgals3*
835 (oligo pair *Lgals3*_del_For-*Lgals3*_del_Rev) were annealed and ligated to linearized vector to
836 generate pX459-*Mpp1*_exon1 and pX-459-*Lgals3*_exon2. Resulting plasmids were sequenced
837 using the primer U6_CRISPR_Seq2 to verify the correct ligation of the vector and targeting
838 oligos. RAW264.7 macrophages were plated overnight and transfected with 3.5µg of each
839 plasmid using Lipofectamine LTX with PLUS reagent (Life Technologies). Puromycin selection
840 (7.5µg/ml) was started 24h after transfection, stopped 24h. After 4-5 days, single-cell cultures
841 were made and individual colonies picked after 10 days for sequencing (*Mpp1*_Seq and
842 *Lgals3*_Seq). Lack of *Mpp1* and *Lgals3* expression was validated by WB.

843

844 ***In vitro* bacterial growth assays**

845 Bacteria were cultured in LB medium or minimal salts medium M63 at 37°C or 32°C (pSIM8)
846 for the indicated times. LB medium was supplemented with DMSO, or heme plus deferoxamine
847 (DFO) where indicated. M63 medium was supplemented with $FeSO_4$ (1.8µM), or 30µM heme
848 plus 200µM 2,2'-bipyridyl (bip) to chelate residual iron. Bacteria were enumerated by plating
849 serial dilutions on blood-agar plates.

850

851 **Bacterial killing assay**

Bacterial killing assays were performed as described earlier[64] using adherent RAW264.7 macrophages ($2.5x10^5$) that were incubated with mid-log phase *E. coli* PMV1 at MOI 80. Serial dilutions of lysates were plated on blood agar plates to quantify viable CFU, the percentage of killed bacteria was calculated: (CFU (t=0min) – CFU (t=x)).

Phagocytosis, efferocytosis assays

Phagocytosis and efferocytosis assays were done essentially as described earlier[65]. To assess bacterial phagocytosis, $2.5\text{-}5x10^5$ respective macrophage subsets were allowed to adhere for 3h. $5x10^5$ human and mouse neutrophils were placed in round bottom tubes in RPMI-1640. All cells were pretreated with DMSO or heme (15min) after which FITC-labeled heat-killed *E. coli*, *S. pneumoniae* or *P. aeruginosa* were added (MOI 100) and incubated at 37°C for 0.5-1h (except where indicated). For neutrophils, FITC-labeled *E. coli* PMV-1 were pre-opsonized with 15% autologous serum. Negative controls were incubated at 4°C during the same period. Adherent macrophages were washed and incubated with proteinase K (50µg/ml) at 4°C to remove adherent bacteria, neutrophils were incubated with trypan blue to quench fluorescence of non-internalized bacteria. Uptake of bacteria was assessed via flow cytometry, the phagocytosis index was calculated as (MFI × % positive cells at 37°C) minus (MFI × % positive cells at 4°C).

Efferocytosis was assessed essentially as above and described earlier[65] using RAW264.7 macrophages and CFSE-labelled apoptotic thymocytes (MOI 10) that were incubated at 37°C for 1h, and stained with CD11c-APC. Uptake of apoptotic cells was analyzed via flow cytometry (FACScalibur), and calculated as $(\text{MFI} \times \%\text{CD11c}^+, \text{CFSE}^+ \text{ cells at } 37°\text{C}) - (\text{MFI} \times \%\text{CD11c}^+, \text{CFSE}^+ \text{ cells at } 4°\text{C})$. FITC-labeled bacteria and CFSE-labeled apoptotic cells were prepared as described earlier[65].

For human whole blood phagocytosis assays, venous blood was collected from healthy donors into EDTA tubes and used as described[66]. Briefly, 100µl undiluted blood was placed in sterile 5ml tubes and DMSO, heme or phenylhydrazine (125µg/g) added for 15min, followed by FITC-labeled *E. coli* (MOI 50) for 20min. To assess the background FITC-fluorescence from non-internalized bacteria cytochalasin D was added (10µM) to control tubes. Erythrocytes were lysed using erythrocyte lysis buffer (Qiagen) and cells were stained with Alexa Fluor 700-CD11b andanalyzed via flow cytometry. Neutrophils and monocytes were identified as $CD11b^+$, SSC^{high} and $CD11b^+$, SSC^{low} cells, respectively. The phagocytosis index was calculated as ((MFI × % positive cells) minus (MFI × % positive cells from cytochalasin D treated tubes)).

To test the uptake of live *L. monocytogenes*, adherent BMDM were pre-treated with 10µM heme or DMSO for 15 min before adding live *L. monocytogenes* (MOI 10) for 1h, followed by gentamycin treatment to kill non-internalized bacteria. Cell lysates were plated on Oxford-Agar plates and the colonies counted the next day.

Confocal phagocytosis and binding assay

Phagocytosis was additionally measured using confocal microscopy. $5x10^4$ macrophages were seeded on 8-well chambers (µ-slide, Ibidi) and allowed to adhere overnight. The cells were treated with DMSO or heme for 15min, and in some experiments pretreated for 45min with mock (PBS) or quinine. FITC-labeled *E. coli* were added (MOI 100) at 37°C for 1h, negative controls (and for bacterial binding analysis) were kept at 4°C. The cells were then washed, fixed with 4% paraformaldehyde, permeabilized with 1% BSA, 0.1% Triton X-100 and stained with DAPI (1µg/ml, Sigma) and phalloidin (0.2µg/ml) conjugated to either TRITC or Alexa Fluor 633. Where indicated, CellMask™ Orange was used at 0.5µg/ml instead of phalloidin. Four to eight random fields per condition were imaged using a confocal microscope (LSM700, Zeiss) with a Plan-Apochromat 20x/0.8 M27 objective. Automatic image analysis was performed using the CellProfiler software[67] (http://www.cellprofiler.org/) which was programed to: a) split images into DAPI, Phalloidin and FITC channels; b) load the channels into the pipeline and identify primary objects (nuclei, DAPI) using Otsu adaptive method with 2-class thresholding, minimized weighted variance and shape method to distinguish clumped objects; c) identify secondary objects (cytoplasm, TRITC or AF633) based on the primary objects (nuclei) identified before using the propagation method with 2-class Otsu global thresholding and minimized weighted variance; d) identify primary objects (bacteria, FITC) using the Otsu global method with 2-class thresholding; e) retrieve only the bacteria present within the cytoplasm of cells. Primary and secondary objects touching the image borders are excluded from analysis. The level of phagocytosis is expressed as the number of internalized bacteria per cell.

***In vivo* phagocytosis assay**

Phagocytosis was assessed *in vivo* as described earlier[68]. WT mice were treated i.p. with PBS or heme (25 µmol/kg body weight) 30min prior to i.p. injection of heat-killed FITC-labeled *E. coli* ($5x10^7$). Peritoneal lavage fluid was harvested 90min later and exudate cells stained for flow cytometry (LSRFortessa). The percentage of $FITC^+$ macrophages ($F4/80^+$, $CD11b^+$, $Ly6G^-$,

913 $CD3^-$, $B220^-$) was assessed as a measure of bacterial uptake and compared to background $FITC^+$
914 B-cells ($CD3^-$, $CD11b^-$, $Ly6G^-$, $F4/80^-$, $B220^+$).

915

916

917 **Cell death and viability assays**

918 Cell death was assessed via LDH release using the CytoTox 96® Non-Radioactive Cytotoxicity
919 kit (Promega) according to instructions from the manufacturer. Cell viability was assessed via the
920 neutral red assay[69]. Briefly, $7.5x10^4$ adherent RAW264.7 macrophages were treated with DMSO,
921 heme or staurosporine (10μM; positive control) in RPMI for the indicated time points and cell
922 viability was calculated as the percentage of the DMSO control absorbance for each treatment
923 and time point.

924

925 **Affinity purification**

926 Affinity chromatography using commercially available hemin-agarose was performed as reported
927 previously[70, 71] using 10 mg RAW264.7 macrophage total cell lysate as protein input in
928 duplicates. Control and heme-competed lysates (pre-incubated lysates with heme) were incubated
929 with beads for 2h at 4°C. Beads were washed extensively with lysis buffer and bound proteins
930 eluted with formic acid. After elution, enriched proteins were reduced with dithiothreitol,
931 cysteine residues alkylated by incubation with iodoacetamide and the samples digested with
932 modified porcine trypsin (Promega, Madison, WI). Three percent (and multiples thereof) of the
933 digested eluates were purified and concentrated by C18 reversed-phase material for subsequent
934 duplicate analysis by gel-free one-dimensional liquid chromatography mass spectrometry (1D-
935 LCMS). Details of the LCMS methodology are as previously described[72].

936

937 **Protein identification**

938 Peak extraction and conversion of RAW files into the MGF format for subsequent protein
939 identification was performed with msconvert (ProteoWizard Library v2.1.2708). An initial
940 database search was performed with broader mass tolerance to re-calibrate the mass lists for
941 optimal final protein identification. For the initial protein database search, Mascot

(www.matrixscience.com, version 2.3.02) was used. Error tolerances on the precursor and fragment ions were ±10 ppm and ±0.6 Da, respectively, and the database search limited to fully-tryptic peptides with maximum 1 missed cleavage, carbamidomethyl cysteine and methionine oxidation set as fixed and variable modifications, respectively. The Mascot peptide ion score threshold was set to 30, and at least 3 peptide identifications per protein were required. Searches were performed against the murine UniProtKB/SwissProt database (www.uniprot.org release 2012-05) including all protein isoforms.

The initial peptide identifications were used to deduce independent linear transformations for precursor and fragment masses that would minimize the mean square deviation of measured masses from theoretical. Re-calibrated mass list files were searched against the same murine protein database by a combination of Mascot and Phenyx (GeneBio, SA, version 2.5.14) search engines using narrower mass tolerances (±4 ppm and ±0.3 Da). One missed tryptic cleavage site was allowed. Carbamidomethyl cysteine was set as a fixed modification and oxidized methionine was set as a variable modification. To validate the proteins, Mascot and Phenyx output files were processed by internally-developed parsers. Proteins with ≥2 unique peptides above a score T1, or with a single peptide above a score T2 were selected as unambiguous identifications. Additional peptides for these validated proteins with score > T3 were also accepted. For Mascot searches, the following thresholds were used: T1=14, T2=40 and T3=10; Phenyx thresholds were set to 4.2, 4.75 and 3.5, respectively (P-value < 10-3). The validated proteins retrieved by the two algorithms were merged, any spectral conflicts discarded and grouped according to shared peptides. A false discovery rate (FDR) of <1% for protein identifications and <0.1% for peptides (including the ones exported with lower scores) was determined by applying the same procedure against a database of reversed protein sequences.

Scoring of identified proteins

Analysis of heme-binding proteins identified by affinity purification and mass spectrometry was performed using the SAINT and CRAPome database bioinformatic tools[32, 33] using empty beads (E.B.) and heme beads, competed with free heme (H.B.C.) as controls. The probability distribution for the calculated CRAPome database scores was inverted to represent the likelihood of each interactor being a contaminant. Gene ontology analysis (DAVID)[73, 74] was used to select a subset of heme-binding proteins involved in the regulation of the actin cytoskeleton, cell and

plasma membrane shape, motility, phagocytosis, and related terms. The resulting list was used for network analysis of interactions using the STRING database v9.1[34].

Automated chemical screen of phagocytosis

A panel of chemicals and drugs was tested using an automated high-throughput analysis of bacterial phagocytosis. Plate handling was performed using the cell::explorer platform (PerkinElmer). Briefly, $5x10^3$ RAW264.7 macrophages were seeded on 384-well clear-bottom plates (4ti-0201 Vision plate™, 4titude), allowed to adhere overnight, and a panel of compounds was transferred using an acoustic dispenser (Echo 520, Labcyte Inc.) at a final concentration of 10µM each and incubated for 3h at 37°C. Each condition was run in triplicates and each plate included 32 DMSO (compound) control wells. Each plate layout was prepared twice with one plate treated for 15min with DMSO (heme control) and the other with 10µM heme (see **Supplementary Fig. 8a** for details). FITC-labeled heat-killed *E. coli* were added (MOI 100) for 1h at 37°C, and washed twice to remove adherent bacteria. Then cells were fixed (4% PFA), permeabilized and stained with DAPI (1µg/ml), phalloidin-TRITC (0.2µg/ml) and imaged using automated fluorescence microscopy with a LUCPlanFLN 20X NA=0.45 objective (Operetta, PerkinElmer) and 5 random fields per well were acquired. The Harmony software (PerkinElmer) was then programmed to analyze each image by: a) Find nuclei in the DAPI channel using the M method; b) Find cytoplasm in the TRITC channel from the nuclei identified before using the A method; c) Find spots (bacteria) in the FITC channel within the cytoplasm identified before using the A method; d) calculate the number of spots (bacteria) identified per cell. The phagocytosis (bacteria/cell) from each image were compiled into matching wells and mean and median phagocytosis data from each compound was normalized to its respective plate control (DMSO or heme). The normalized values were $\log_2$ transformed to obtain the $\log_2$ fold change of phagocytosis induced by each compound in the presence of DMSO or heme. To score the tested compounds (C-Score), the following formula was employed:

$$C\text{-}Score = \frac{log_2\ fold\ change(mean\ or\ median)_{Heme}}{1 + |log_2\ fold\ change\ (mean\ or\ median)_{DMSO}|}$$

The resulting C-Scores obtained from mean or median values of phagocytosis for each compound were plotted against each other to estimate the data noise (**Supplementary Fig. 8b**). Compounds with $\log_2$ mean fold change (over heme) of phagocytosis>0.75 and C-Scores>0.5 were considered as significantly restoring phagocytosis. Additionally, compounds for which the C-Scores differed by more than 30% from the calculated linear regression were excluded (**Supplementary Fig. 8b**).

Cdc42 activation assay

The activation of Cdc42 was assessed using the Cdc42 G-LISA Activation Assay (Colorimetric format) kit as indicated by the manufacturer (#BK127, Cytoskeleton, Inc.). Briefly, adherent RAW264.7 or HoxB8 macrophages were serum-starved for 2h before DMSO or heme was added for the indicated time points. Active Cdc42 signal was measured according to the instructions by the manufacturer and corrected for protein content.

Microscopy, image analysis and live cell imaging

For cell shape analysis, RAW264.7 macrophages, BMDM, human monocyte-derived macrophages and HoxB8 macrophages were seeded on 8-chamber slides (µ-slide, Ibidi) at a density of $5x10^4$ per well and allowed to adhere overnight. The cells were washed twice with PBS and, where indicated, pretreated in RPMI with ML-141, CK666 or K216-0385 for 1h, or *N*-acetyl-*L*-cysteine (NAC) for 30min. Where indicated, ML-141 was washed away after pretreatment and the cells were allowed 15min to recover. The cells were then treated with DMSO, heme or bradykinin for 15 to 30min. For calcium-influx experiments, the cells were treated with DMSO or heme for 15min in DMEM or in DMEM lacking calcium (LifeTech). After stimulation, cells were fixed with 4% PFA and stained with DAPI (1µg/ml) and phalloidin-FITC or phalloidin-TRITC (0,2µg/ml). Four to eight random fields per well were acquired using a Zeiss LSM700 confocal microscope equipped with a Plan-Apochromat 20x/0.8 M27 objective. The images were loaded into the CellProfiler image analysis software and the pipeline was programmed to retrieve the cell shape parameters for the cell area, perimeter and form factor (circularity) as described earlier[56]. For 3D cell reconstruction Z-stacks were acquired using a Zeiss LSM780 confocal microscope equipped with a Plan-Apochromat 100x/1.4 Oil DIC M27 objective,. Each slice was then deconvolved using Huygens Professional (Scientific Volume

Imaging) and the corresponding theoretical point spread function. The deconvolved Z-stacks were then used to generate 3D animations of the cells using Huygens Professional SFP renderer module.

Live cell imaging of the actin cytoskeleton was performed using the LifeAct-GFP fusion construct[75] to generate LifeAct-GFP positive RAW264.7 macrophages ($RAW^{LifeAct\text{-}GFP}$). These were plated at a density of $7{,}5x10^4$ cells/dish, allowed to adhere and stained with Hoechst 33258 (5µg/ml). Immediately before time-lapse image acquisition, DMSO, heme or PPIX (10µM) were added and cells were imaged every 25s for 60 to 80 frames using a Zeiss LSM780 confocal microscope equipped with a Plan-Apochromat 40x/1.3 DIC M27 objective and an incubator chamber maintaining 37°C and 5% CO_2.

Migration assays

BMDM motility was assessed using a wound-healing (scratch) assay. WT BMDM were seeded to near confluency onto 12-well plates ($5x10^5$ cells/well) and allowed to adhere for 3h. The adherent confluent cell layer was scratched using a 10µl pipette tip and the cells washed twice to remove the cell debris. The cells were treated for 15min with DMSO or heme (3 to 30µM) in RPMI-1640 and images of the scratches were collected at the indicated time points using phase-contrast on a DMI6000B inverted microscope (Leica) equipped with an N-Plan 10.0x-0.25 objective and a motorized xyz-stage. The images were loaded into CellProfiler software and image illumination correction functions were applied to each image. The intensity of the corrected images was normalized using ImageJ (v1.47) and the images loaded into the scratch assay analysis software TScratch[76]. The remaining open areas were used to calculate the percentage of the initial open area, which the cells occupy at the different time points.

Cell movement towards a chemokine gradient was performed on collagen gel matrices. Mature BMDC were treated with DMSO or heme at the indicated concentrations in RPMI-1640 and $1.2x10^6$ cells/ml were mixed with the collagen gel mix (1.6mg/ml bovine collagen I, 3.5mM $NaHCO_3$ and 1X MEM final concentrations) at a ratio of 2:1. The gel mix containing the cells were introduced into custom-made migration chambers (2mm thick) and incubated for 45min to allow the gel to polymerize. The polymerized gel chambers were overlaid with CCL19 (250ng/ml in RPMI-1640, 10%FCS, 1%P/S) and gel images for each condition were simultaneously taken

every 2min for 6h using a Zeiss Axiovert 40 CFL inverted microscope equipped with custom-built climate chambers (5% CO_2, 37 °C, humidified). The image stacks were loaded into the FiJi image analysis software[77] and individual cell movement was tracked using a custom plugin to calculate the cell migration index. Track coordinates were introduced onto Ibidi Chemotaxis and Migration tool (http://ibidi.com/software/chemotaxis_and_migration_tool/) to retrieve centered coordinates and track directionality. Math software R (https://www.r-project.org/) with ggplot2 package (https://cran.r-project.org/web/packages/ggplot2/index.html) were then used to render both the track distance and wind rose plots.

Cell adhesion and rolling

Sterile Cellix Vena8 Endothelial+™ Biochip capillaries were coated overnight with FNC coating mix® (Athena enzyme). Immortalized human microvascular endothelial cells (G1S1) were seeded into each capillary and grown to confluence for 24h at 37°C under flow (400 µl/min) in EGM-2-MV medium containing 10ng/ml human TNF. Biochips were then attached to the Cellix Nanopump 2.0 and flushed with EGM-2-MV at 8 Dynes/cm^2. 50µl of DMSO- or heme-treated (15min) human monocyte cell suspensions (3.5x10^6/ml) were loaded into the biochips and images were acquired with an inverted microscope (Zeiss Axiovert 200M) equipped with a CCD camera (Zeiss Axiocam MRc5) every second for 2min with an exposure time of 344ms. Image sequences were analyzed for cell adhesion and rolling with the cell-tracking tool of Image Pro Plus software.

PCR and Western blot

PCR was performed using Taq DNA polymerase, dNTPack (Roche life sciences), High Fidelity PCR Enzyme Mix (Thermo scientific) or Phusion High-Fidelity DNA polymerase (Thermo Scientific) according to instructions from the manufacturers. Primer sequences are indicated in **Supplementary Table 3**. For Western blot analysis, cell lysates were prepared in RIPA buffer, mixed 1:1 with 2x SDS sample buffer and boiled for 5min at 99°C. Cell lysates or pull-down eluates were resolved in polyacrylamide gels, blotted onto PVDF membranes, and incubated overnight at 4°C with anti-DOCK8, LGALS3, MPP1, ATP6V1A, ARPC3 antibodies (1:750), anti-CDC42 antibody (1:500) or anti-ACTB antibody (1:1000), followed anti-rabbit IgG-HRP (1:1000) or goat anti-mouse IgG (H+L)-HRP (1:3000) and Amersham ECL Western Blotting

Detection Reagent prior to developing. Some membranes were stripped using stripping buffer, washed and further stained as above.

Statistical analysis

Comparisons between groups were performed using unpaired, two-sided *t*-test for normally distributed data, or Mann-Whitney otherwise. For grouped comparisons, one-way or two-way ANOVA followed by Tukey's multiple comparisons analysis were used where appropriate. Data correlation was assessed using the Pearson product-moment correlation coefficient. Sample sizes for *in vivo* experiments were calculated based on previous experience using the Power/sample-size calculator (http://www.stat.ubc.ca/~rollin/stats/ssize/n2.html). Statistically significant outliers were assessed using Grubb's test (alpha = 0.05) and were excluded from analysis. Animal studies were performed without prior randomization or blinding. Survival data was analyzed by Log rank (Mantel-Cox) test using GraphPad Prism v6.07 Software. Data is presented as mean ± S.E.M. except where indicated.

Supplementary References

32. Choi, H. *et al.* SAINT: probabilistic scoring of affinity purification-mass spectrometry data. *Nat Methods* **8**, 70-73 (2011).

33. Mellacheruvu, D. *et al.* The CRAPome: a contaminant repository for affinity purification-mass spectrometry data. *Nat Methods* **10**, 730-736 (2013).

34. Franceschini, A. *et al.* STRING v9.1: protein-protein interaction networks, with increased coverage and integration. *Nucleic acids research* **41**, D808-815 (2013).

44. Krishnaswamy, J.K. *et al.* Coincidental loss of DOCK8 function in NLRP10-deficient and C3H/HeJ mice results in defective dendritic cell migration. *Proc Natl Acad Sci U S A* **112**, 3056-3061 (2015).

48. Mobley, H.L. *et al.* Pyelonephritogenic Escherichia coli and killing of cultured human renal proximal tubular epithelial cells: role of hemolysin in some strains. *Infection and immunity* **58**, 1281-1289 (1990).

49. Sharan, S.K., Thomason, L.C., Kuznetsov, S.G. & Court, D.L. Recombineering: a homologous recombination-based method of genetic engineering. *Nature protocols* **4**, 206-223 (2009).

50. Sewnath, M.E. *et al.* IL-10-deficient mice demonstrate multiple organ failure and increased mortality during Escherichia coli peritonitis despite an accelerated bacterial clearance. *Journal of immunology* **166**, 6323-6331 (2001).

51. Peris-Bondia, F., Muraille, E. & Van Melderen, L. Complete Genome Sequence of the Escherichia coli PMV-1 Strain, a Model Extraintestinal Pathogenic E. coli Strain Used for Host-Pathogen Interaction Studies. *Genome Announc* **1** (2013).

52. McKenzie, G.J. & Craig, N.L. Fast, easy and efficient: site-specific insertion of transgenes into enterobacterial chromosomes using Tn7 without need for selection of the insertion event. *BMC microbiology* **6**, 39 (2006).

53. Ran, F.A. *et al.* Genome engineering using the CRISPR-Cas9 system. *Nature protocols* **8**, 2281-2308 (2013).

54. Gauvin, T.J., Fukui, J., Peterson, J.R. & Higgs, H.N. Isoform-selective chemical inhibition of mDia-mediated actin assembly. *Biochemistry* **48**, 9327-9329 (2009).

55. Redecke, V. *et al.* Hematopoietic progenitor cell lines with myeloid and lymphoid potential. *Nat Methods* **10**, 795-803 (2013).

56. Matt, U. *et al.* WAVE1 mediates suppression of phagocytosis by phospholipid-derived DAMPs. *J Clin Invest* **123**, 3014-3024 (2013).

57. Ploplis, V.A., French, E.L., Carmeliet, P., Collen, D. & Plow, E.F. Plasminogen deficiency differentially affects recruitment of inflammatory cell populations in mice. *Blood* **91**, 2005-2009 (1998).

58. Kernbauer, E., Maier, V., Rauch, I., Muller, M. & Decker, T. Route of Infection Determines the Impact of Type I Interferons on Innate Immunity to. *PLoS One* **8**, e65007 (2013).

59. Stockinger, S. *et al.* Characterization of the interferon-producing cell in mice infected with Listeria monocytogenes. *PLoS Pathog* **5**, e1000355 (2009).

60. Huy, N.T. *et al.* An improved colorimetric method for quantitation of heme using tetramethylbenzidine as substrate. *Analytical biochemistry* **344**, 289-291 (2005).

61. Schenkman, J.B. & Jansson, I. Spectral analyses of cytochromes P450. *Methods Mol Biol* **320**, 11-18 (2006).

62. Grundy, M.A., Gorman, N., Sinclair, P.R., Chorney, M.J. & Gerhard, G.S. High-throughput non-heme iron assay for animal tissues. *J Biochem Biophys Methods* **59**, 195-200 (2004).

63. Cross, M.A., Koronakis, V., Stanley, P.L. & Hughes, C. HlyB-dependent secretion of hemolysin by uropathogenic Escherichia coli requires conserved sequences flanking the chromosomal hly determinant. *Journal of bacteriology* **172**, 1217-1224 (1990).

64. Knapp, S., Matt, U., Leitinger, N. & van der Poll, T. Oxidized phospholipids inhibit phagocytosis and impair outcome in gram-negative sepsis in vivo. *J Immunol* **178**, 993-1001 (2007).

65. Sharif, O. *et al.* The triggering receptor expressed on myeloid cells 2 inhibits complement component 1q effector mechanisms and exerts detrimental effects during pneumococcal pneumonia. *PLoS pathogens* **10**, e1004167 (2014).

66. White-Owen, C., Alexander, J.W., Sramkoski, R.M. & Babcock, G.F. Rapid whole-blood microassay using flow cytometry for measuring neutrophil phagocytosis. *J Clin Microbiol* **30**, 2071-2076 (1992).

67. Carpenter, A.E. *et al.* CellProfiler: image analysis software for identifying and quantifying cell phenotypes. *Genome biology* **7**, R100 (2006).

68. Gawish, R. *et al.* Triggering receptor expressed on myeloid cells-2 fine-tunes inflammatory responses in murine Gram-negative sepsis. *FASEB J* (2014).

69. Repetto, G., del Peso, A. & Zurita, J.L. Neutral red uptake assay for the estimation of cell viability/cytotoxicity. *Nature protocols* **3**, 1125-1131 (2008).

70. Fernbach, N.V. *et al.* Acid elution and one-dimensional shotgun analysis on an Orbitrap mass spectrometer: an application to drug affinity chromatography. *J Proteome Res* **8**, 4753-4765 (2009).

71. Huber, K.V. *et al.* Stereospecific targeting of MTH1 by (S)-crizotinib as an anticancer strategy. *Nature* **508**, 222-227 (2014).

72. Maurer, M. *et al.* Combining Filter-Aided Sample Preparation and Pseudoshotgun Technology To Profile the Proteome of a Low Number of Early Passage Human Melanoma Cells. *Journal of Proteome Research* **12**, 1040-1048 (2012).

73. Huang da, W., Sherman, B.T. & Lempicki, R.A. Systematic and integrative analysis of large gene lists using DAVID bioinformatics resources. *Nature protocols* **4**, 44-57 (2009).

74. Huang da, W., Sherman, B.T. & Lempicki, R.A. Bioinformatics enrichment tools: paths toward the comprehensive functional analysis of large gene lists. *Nucleic acids research* **37**, 1-13 (2009).

75. Riedl, J. *et al.* Lifeact: a versatile marker to visualize F-actin. *Nat Methods* **5**, 605-607 (2008).

76. Geback, T., Schulz, M.M., Koumoutsakos, P. & Detmar, M. TScratch: a novel and simple software tool for automated analysis of monolayer wound healing assays. *BioTechniques* **46**, 265-274 (2009).

77. Schindelin, J. *et al.* Fiji: an open-source platform for biological-image analysis. *Nat Methods* **9**, 676-682 (2012).

Figure 1

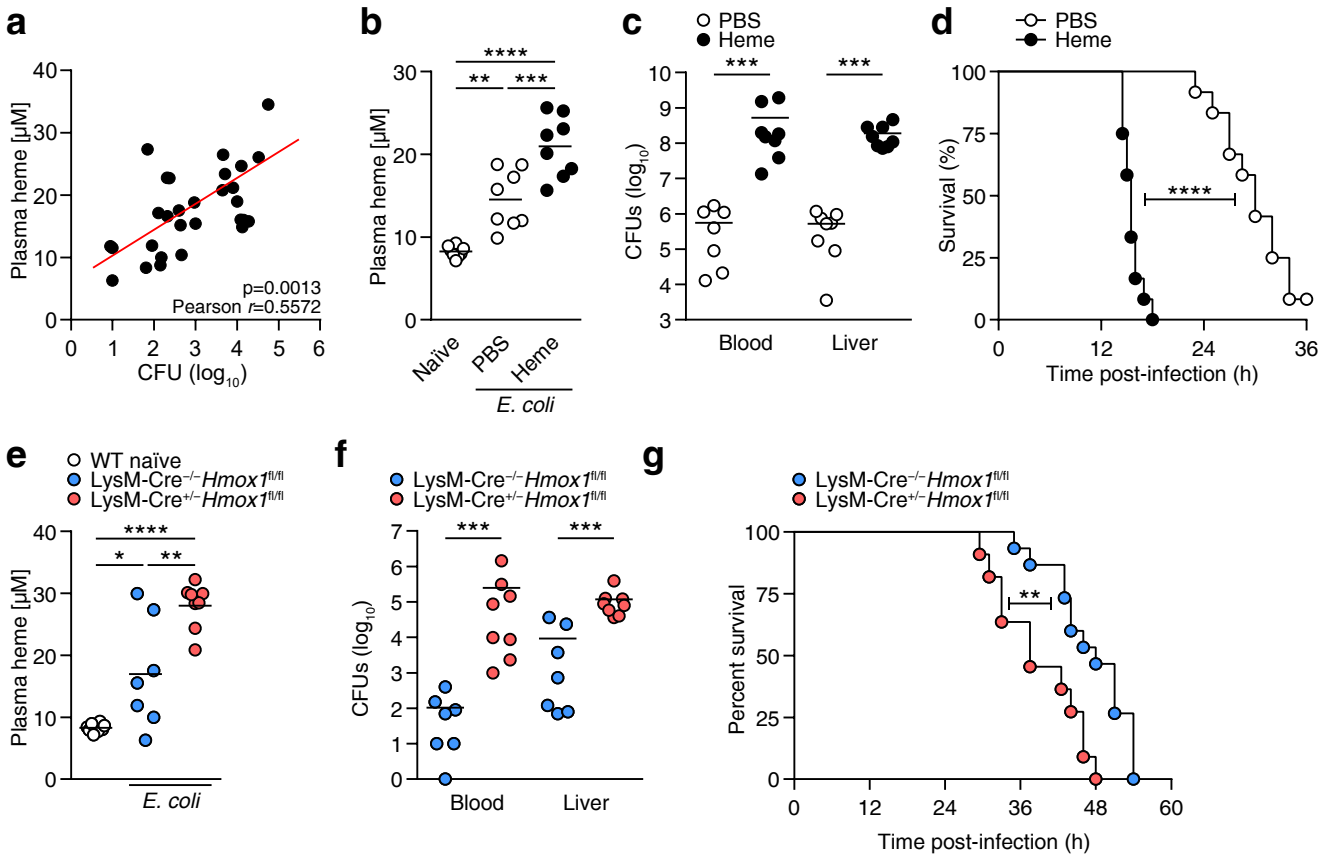
a
Plasma heme [μM]
CFU (log10)
p=0.0013
Pearson r=0.5572
b
Plasma heme [μM]
Naïve
PBS
Heme
E. coli
c
PBS
Heme
CFUs (log10)
Blood
Liver
d
PBS
Heme
Survival (%)
Time post-infection (h)
e
WT naïve
LysM-Cre−/−Hmox1fl/fl
LysM-Cre+/−Hmox1fl/fl
Plasma heme [μM]
E. coli
f
LysM-Cre−/−Hmox1fl/fl
LysM-Cre+/−Hmox1fl/fl
CFUs (log10)
Blood
Liver
g
LysM-Cre−/−Hmox1fl/fl
LysM-Cre+/−Hmox1fl/fl
Percent survival
Time post-infection (h)

Figure 2

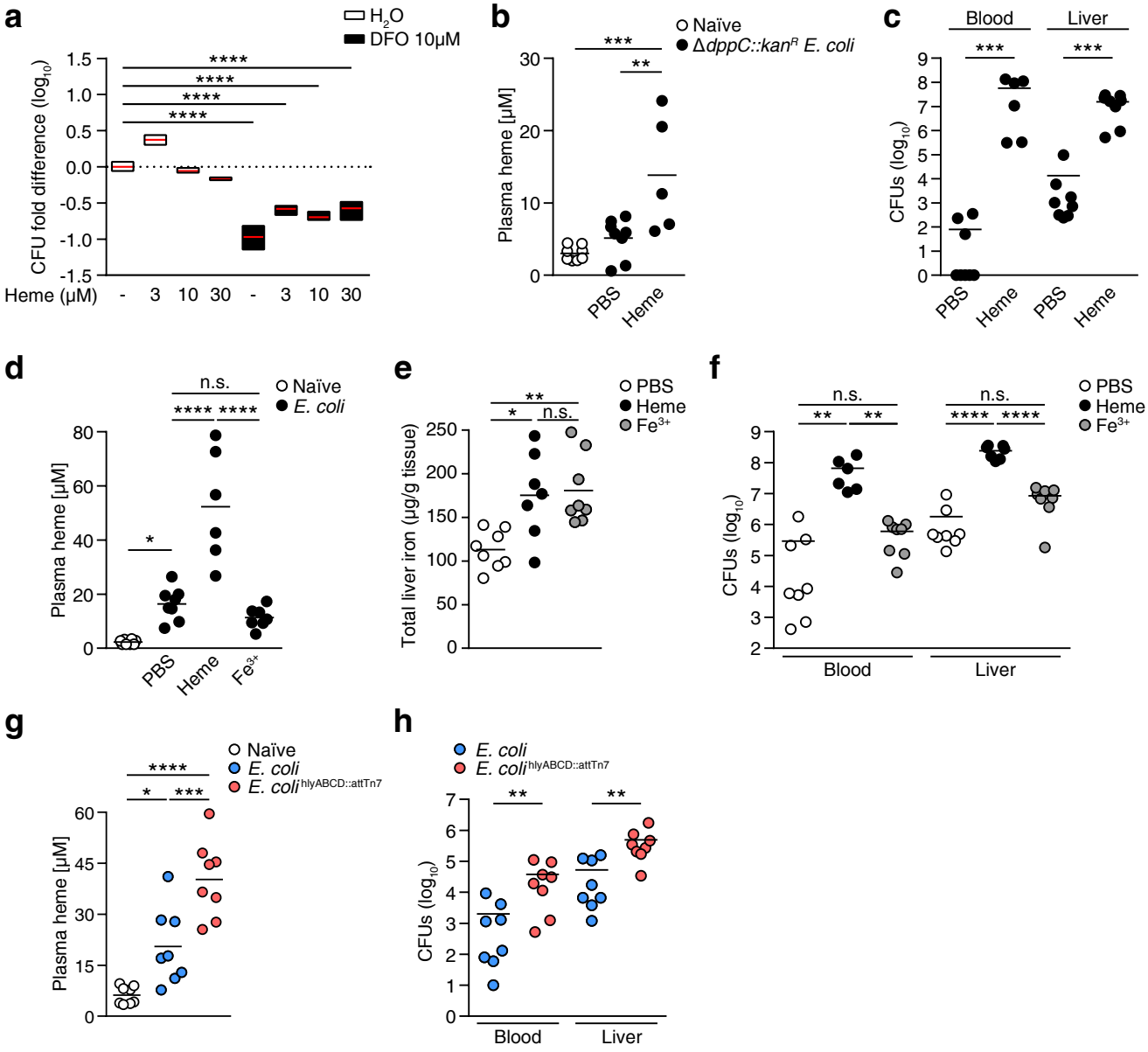
a
H2O
DFO 10μM
CFU fold difference (log10)
Heme (μM)
b
Naïve
ΔdppC::kanR E. coli
Plasma heme [μM]
PBS
Heme
c
Blood
Liver
CFUs (log10)
d
Naïve
E. coli
Plasma heme [μM]
PBS
Heme
Fe3+
e
PBS
Heme
Fe3+
Total liver iron (μg/g tissue)
f
PBS
Heme
Fe3+
CFUs (log10)
Blood
Liver
g
Naïve
E. coli
E. coli hlyABCD::attTn7
Plasma heme [μM]
h
E. coli
E. coli hlyABCD::attTn7
CFUs (log10)
Blood
Liver

Figure 3

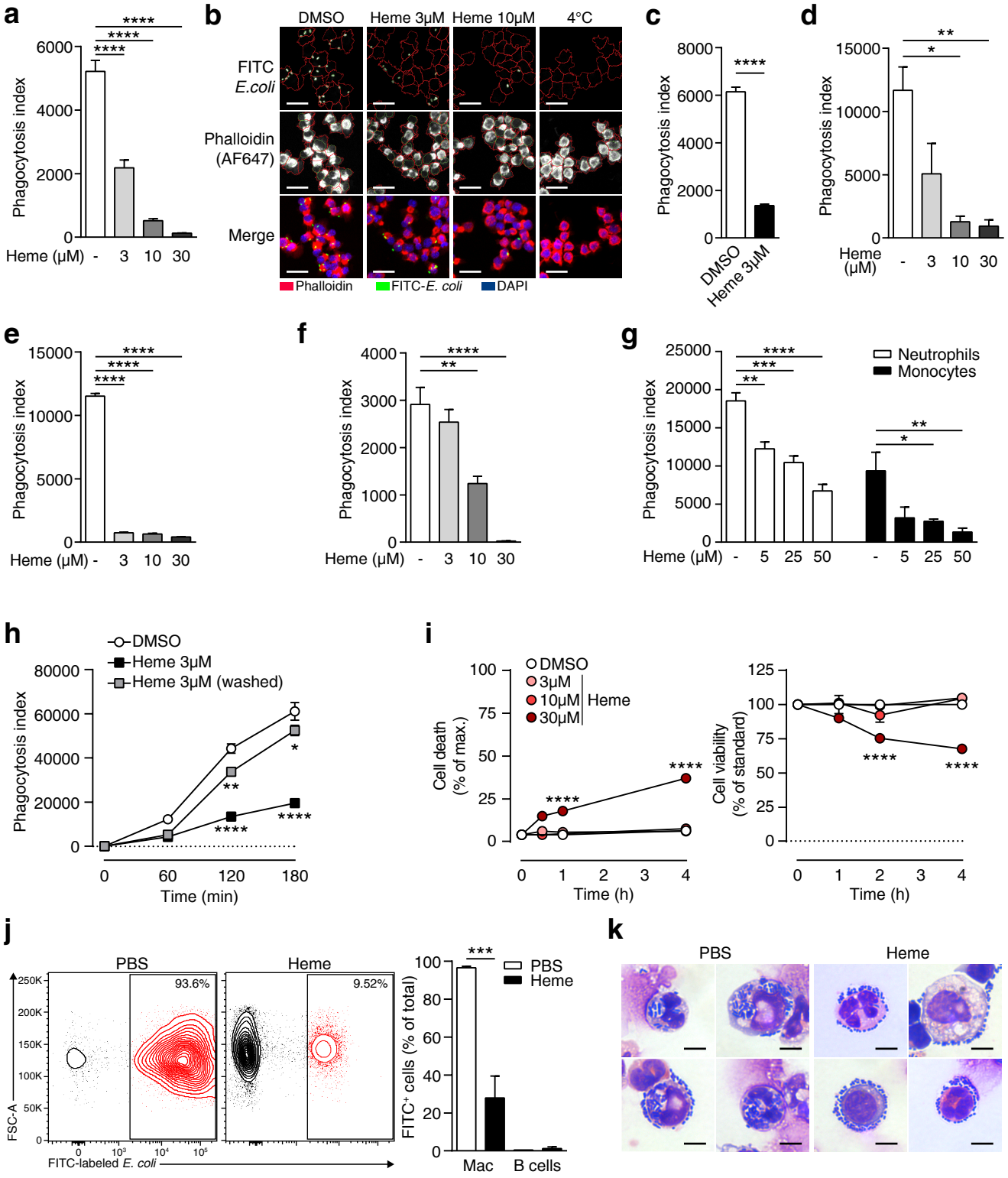
a
Phagocytosis index
Heme (μM) - 3 10 30
b
DMSO
Heme 3μM
Heme 10μM
4°C
FITC E.coli
Phalloidin (AF647)
Merge
Phalloidin
FITC-E. coli
DAPI
c
Phagocytosis index
DMSO
Heme 3μM
d
Phagocytosis index
Heme (μM) - 3 10 30
e
Phagocytosis index
Heme (μM) - 3 10 30
f
Phagocytosis index
Heme (μM) - 3 10 30
g
Phagocytosis index
Neutrophils
Monocytes
Heme (μM) - 5 25 50 - 5 25 50
h
DMSO
Heme 3μM
Heme 3μM (washed)
Phagocytosis index
Time (min)
i
DMSO
3μM
10μM
30μM
Heme
Cell death (% of max.)
Time (h)
Cell viability (% of standard)
Time (h)
j
PBS
Heme
93.6%
9.52%
FSC-A
FITC-labeled E. coli
FITC+ cells (% of total)
PBS
Heme
Mac
B cells
k
PBS
Heme

Figure 4

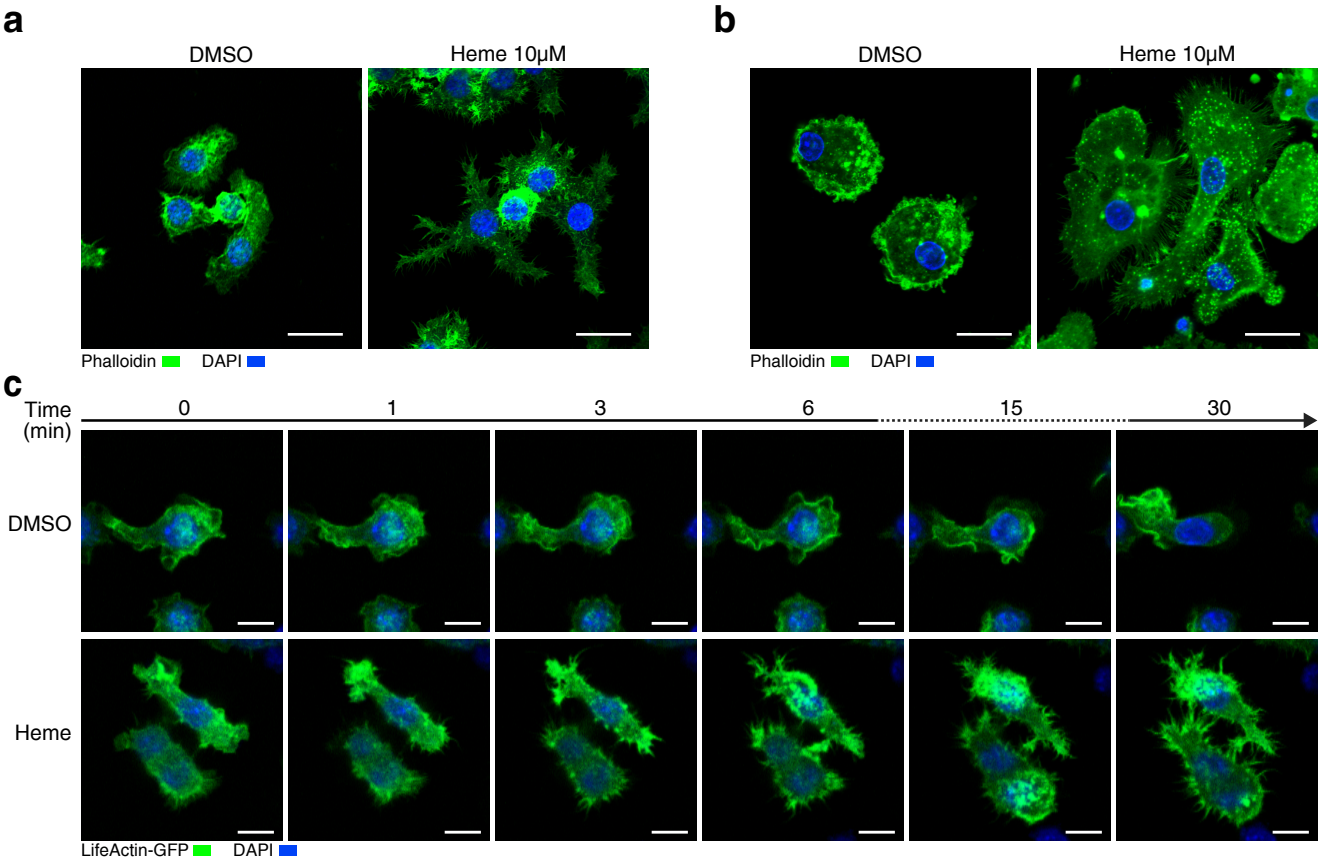
a
DMSO
Heme 10μM
Phalloidin
DAPI
b
DMSO
Heme 10μM
Phalloidin
DAPI
c
Time (min)
0
1
3
6
15
30
DMSO
Heme
LifeActin-GFP
DAPI
d
DMSO
Heme 3μM
Heme 10μM
Cell area (μm²)
Form factor (Perfect circle=1)
Heme (μM)
e
DMSO
Heme 3μM
Heme 10μM
Cell area (μm²)
Form factor (Perfect circle=1)
Heme (μM)

Figure 5

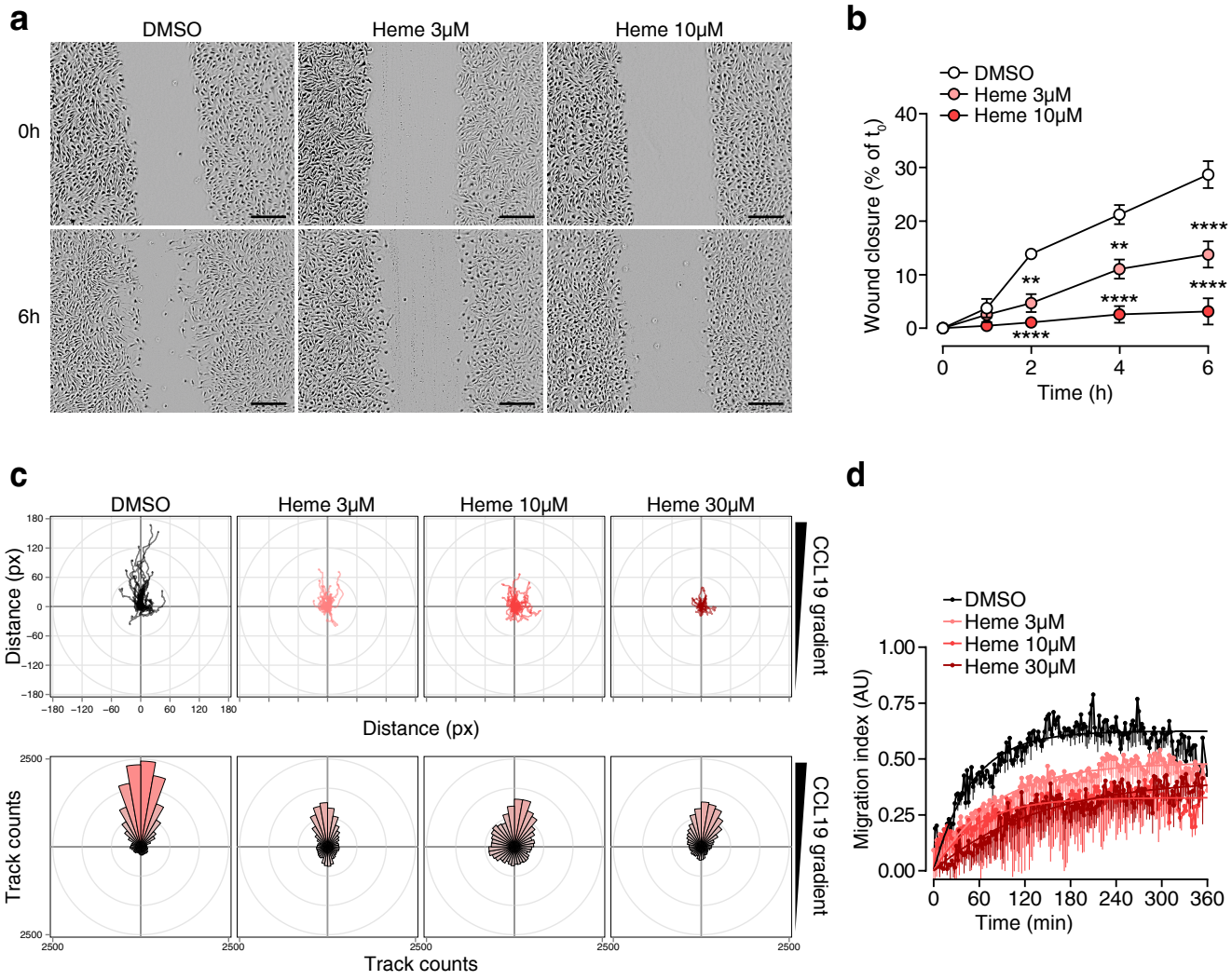
a
DMSO
Heme 3μM
Heme 10μM
0h
6h
b
DMSO
Heme 3μM
Heme 10μM
Wound closure (% of t0)
Time (h)
c
DMSO
Heme 3μM
Heme 10μM
Heme 30μM
Distance (px)
Track counts
CCL19 gradient
d
DMSO
Heme 3μM
Heme 10μM
Heme 30μM
Migration index (AU)
Time (min)

Figure 6

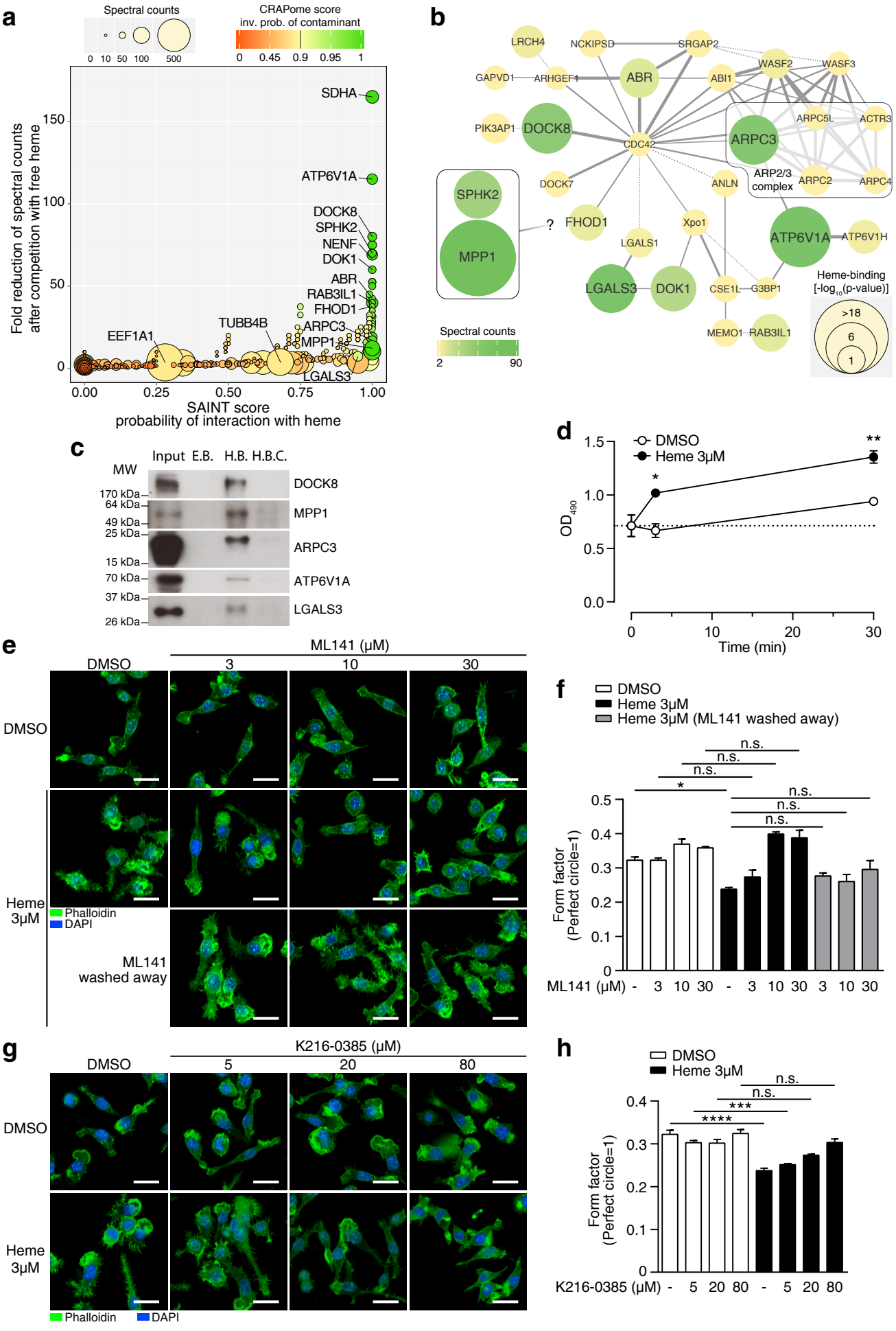
a
Spectral counts
0 10 50 100 500
CRAPome score
inv. prob. of contaminant
0 0.45 0.9 0.95 1
Fold reduction of spectral counts after competition with free heme
SAINT score
probability of interaction with heme
SDHA
ATP6V1A
DOCK8
SPHK2
NENF
DOK1
ABR
RAB3IL1
FHOD1
ARPC3
MPP1
LGALS3
TUBB4B
EEF1A1
b
LRCH4
NCKIPSD
SRGAP2
WASF2
WASF3
GAPVD1
ARHGEF1
ABR
ABI1
PIK3AP1
DOCK8
ARPC5L
ACTR3
CDC42
ARPC3
ARP2/3 complex
ARPC2
ARPC4
DOCK7
ANLN
SPHK2
MPP1
FHOD1
Xpo1
ATP6V1A
ATP6V1H
LGALS1
LGALS3
DOK1
CSE1L
G3BP1
MEMO1
RAB3IL1
Heme-binding
[-log10(p-value)]
>18
6
1
Spectral counts
2 90
c
Input E.B. H.B. H.B.C.
MW
170 kDa
64 kDa
49 kDa
25 kDa
15 kDa
70 kDa
37 kDa
26 kDa
DOCK8
MPP1
ARPC3
ATP6V1A
LGALS3
d
DMSO
Heme 3μM
OD490
Time (min)
e
ML141 (μM)
DMSO
3
10
30
DMSO
Heme 3μM
ML141 washed away
Phalloidin
DAPI
f
DMSO
Heme 3μM
Heme 3μM (ML141 washed away)
Form factor (Perfect circle=1)
ML141 (μM) - 3 10 30 - 3 10 30 3 10 30
n.s.
*
g
K216-0385 (μM)
DMSO
5
20
80
DMSO
Heme 3μM
Phalloidin
DAPI
h
DMSO
Heme 3μM
Form factor (Perfect circle=1)
K216-0385 (μM) - 5 20 80 - 5 20 80
n.s.
***
****

Figure 7

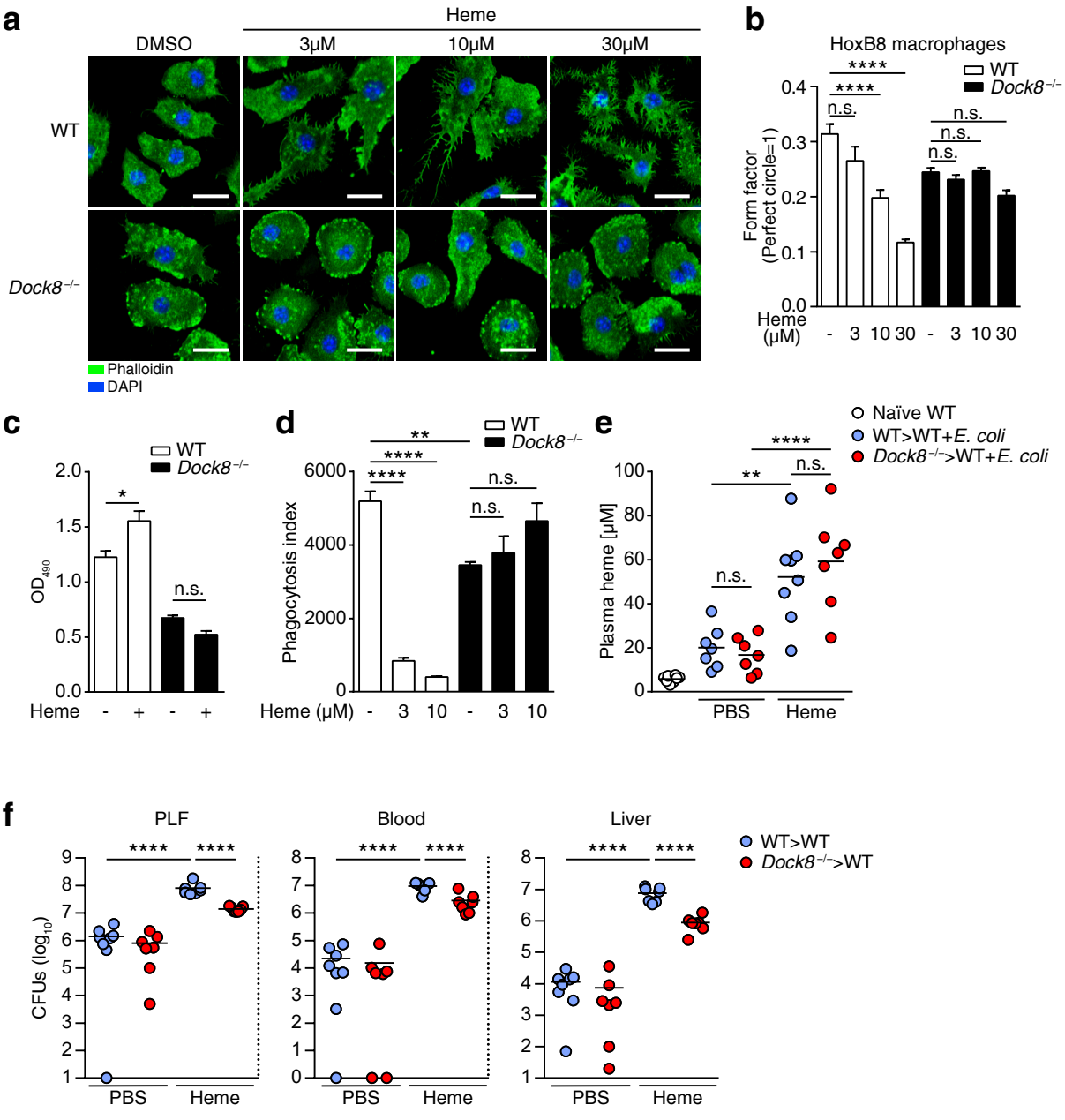
a
Heme
DMSO
3μM
10μM
30μM
WT
Dock8−/−
Phalloidin
DAPI
b
HoxB8 macrophages
WT
Dock8−/−
Form factor (Perfect circle=1)
Heme (μM)
c
WT
Dock8−/−
OD490
Heme
d
WT
Dock8−/−
Phagocytosis index
Heme (μM)
e
Naïve WT
WT>WT+E. coli
Dock8−/−>WT+E. coli
Plasma heme [μM]
PBS
Heme
f
PLF
Blood
Liver
WT>WT
Dock8−/−>WT
CFUs (log10)
PBS
Heme

Figure 8

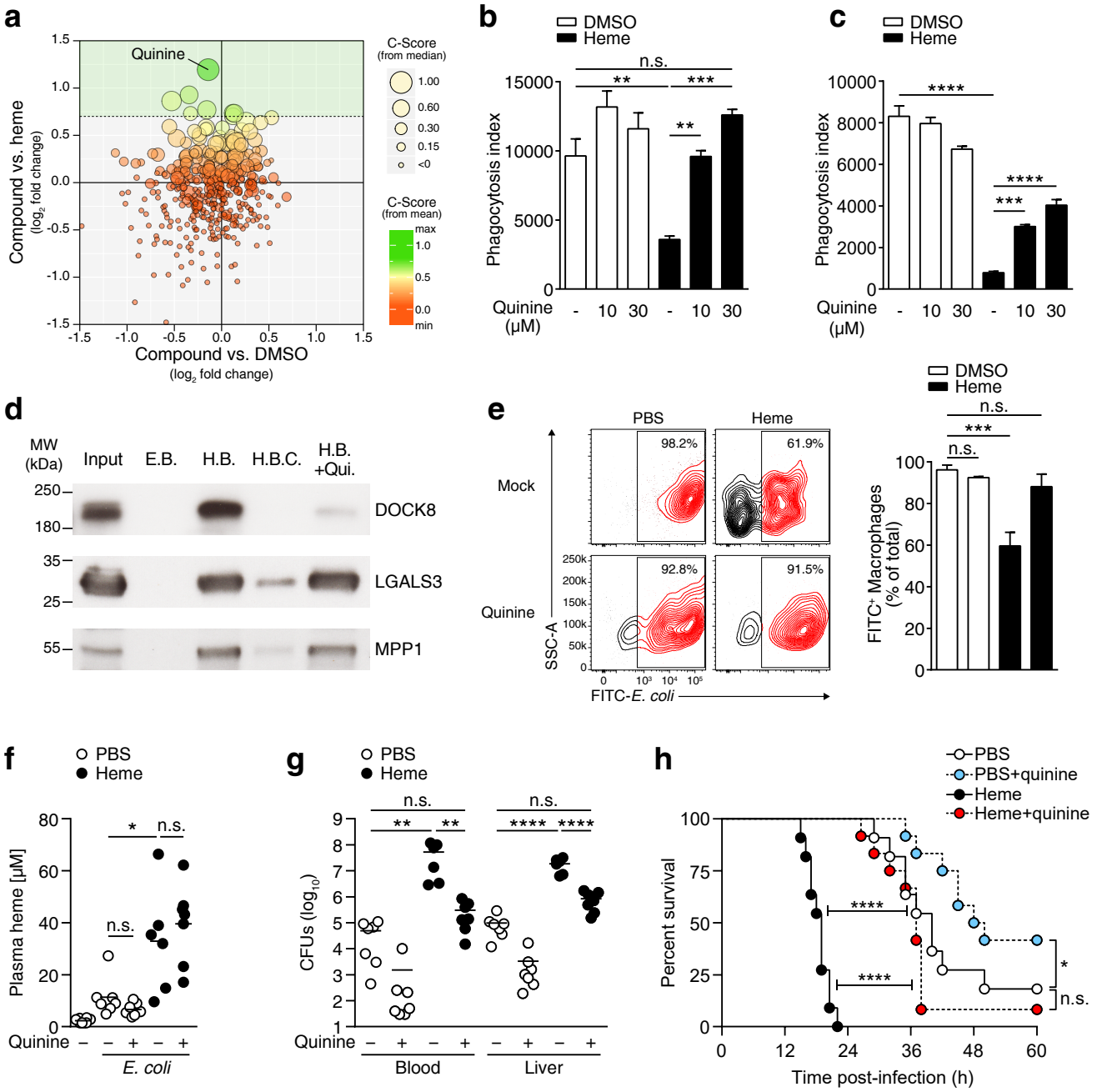
a
Quinine
C-Score (from median)
1.00
0.60
0.30
0.15
<0
C-Score (from mean)
max
1.0
0.5
0.0
min
Compound vs. heme (log2 fold change)
Compound vs. DMSO (log2 fold change)
b
DMSO
Heme
n.s.
**
***
**
Phagocytosis index
Quinine (μM)
- 10 30 - 10 30
c
DMSO
Heme
****
****
***
Phagocytosis index
Quinine (μM)
- 10 30 - 10 30
d
MW (kDa)
Input
E.B.
H.B.
H.B.C.
H.B. +Qui.
DOCK8
LGALS3
MPP1
e
PBS
Heme
Mock
Quinine
98.2%
61.9%
92.8%
91.5%
SSC-A
FITC-E. coli
DMSO
Heme
n.s.
***
n.s.
FITC+ Macrophages (% of total)
f
PBS
Heme
Plasma heme [μM]
*
n.s.
n.s.
Quinine
E. coli
g
PBS
Heme
n.s.
n.s.
**
**
****
****
CFUs (log10)
Quinine
Blood
Liver
h
PBS
PBS+quinine
Heme
Heme+quinine
Percent survival
****
****
*
n.s.
Time post-infection (h)